The Evolution of Seabirds in the Humboldt Current: New Clues from the Pliocene of Central Chile

Chávez Hoffmeister, Martín; Carrillo Briceño, Jorge D; Nielsen, Sven N

Abstract: Unspecified

DOI: 10.1371/journal.pone.0090043

OPEN ACCESS Freely available online

PLOS ONE

The Evolution of Seabirds in the Humboldt Current: New Clues from the Pliocene of Central Chile

Martín Chávez Hoffmeister[1,3]*, Jorge D. Carrillo Briceño[2], Sven N. Nielsen[3]

1 School of Earth Sciences, University of Bristol, Bristol, United Kingdom, **2** Palaeontological Institute and Museum, University of Zürich, Zürich, Switzerland, **3** Instituto de Ciencias Ambientales y Evolutivas, Universidad Austral de Chile, Valdivia, Chile

Abstract

Background: During the last decade, new Neogene fossil assemblages from South America have revealed important clues about the evolution of seabird faunas in one of the major upwelling systems of the world: the Humboldt Current. However, most of this record comes from arid Northern Chile and Southern Peru and, in consequence, our knowledge of the evolutionary history of seabirds in the temperate transitional zone is negligible. A new Late Pliocene assemblage of fossil birds from the coastal locality of Horcon in Central Chile offers a unique opportunity to fill this gap.

Principal Findings: Isolated bones of a medium-sized penguin are the most abundant bird remains. Morphological and cladistic analyses reveal that these specimens represent a new species of crested penguin, *Eudyptes calauina* sp. nov. *Eudyptes* is a penguin genus that inhabit temperate and subantarctic regions and currently absent in central Chile. Additionally, a partial skeleton of a small species of cormorant and a partial tarsometatarsus of a sooty shearwater have been identified.

Conclusion/Significance: The Horcon fossils suggest the existence of a mixed avifauna in central Chile during the Pliocene in concordance with the latitudinal thermal gradient. This resembles the current assemblages from the transitional zone, with the presence of species shared with Northern Chile and Southern Peru and a previously unrecorded penguin currently absent from the Humboldt System but present in the Magellanic region. Comparison of Pliocene seabird diversity across the Pacific coast of South America shows that the Horcon avifauna represents a distinctive assemblage linking the living faunas with the Late Miocene ones. A comparison with the fossil record near the Benguela Current (west coast of southern Africa) suggests that the thermic gradient could play an important role in the preservation of a higher diversity of cold/temperate seabirds in the Humboldt Current.

Citation: Chávez Hoffmeister M, Carrillo Briceño JD, Nielsen SN (2014) The Evolution of Seabirds in the Humboldt Current: New Clues from the Pliocene of Central Chile. PLoS ONE 9(3): e90043. doi:10.1371/journal.pone.0090043

Editor: Laurent Viriot, Team 'Evo-Devo of Vertebrate Dentition', France

Received August 14, 2013; **Accepted** January 28, 2014; **Published** March 12, 2014

Funding: The Dirección de Investigación y Desarrollo (DID) of the Universidad Austral de Chile provided funding to cover part of the Publication Fees of the present paper. The funders had no role in study design, data collection and analysis, decision to publish, or preparation of the manuscript. No additional funding was received for this study.

Competing Interests: The authors have declared that no competing interests exist.

* E-mail: glmfch@bristol.ac.uk

Introduction

The fossil record of seabirds is often abundant in Cenozoic marine formations. Nevertheless, there is a clear asymmetry in our knowledge of fossil seabird communities between the Northern and Southern hemispheres. Of the 368 records of seabirds presented by Warheit [1], only 25% come from the Southern Hemisphere and of those, 27% come from South America. Fortunately, the number of taxa reported for South America had been increasing in abundance and diversity during the last decade, including two of the most important Neogene assemblages: the Late Miocene Bahia Inglesa Formation in northern Chile [2–4], and the Middle Miocene to Pliocene Pisco Formation in Southern Peru [5–7]. These are key areas for the study of the evolution of seabird faunas in one of the major upwelling systems of the world: the Humboldt Current.

The Humboldt Current system [8] is one of the most productive marine ecosystems worldwide and its area of influence defines one of the largest biogeographical provinces in the southern oceans: the Peruvian-Chilean Province (PCP) [9], which has been recognized as one of the main areas of endemism for seabirds in Chile [10]. Some authors also recognize a transition zone at its southern limit, between 30 and 43°S, also known as the Central [11] or Central Chilean Province [12], where this fauna becomes progressively more similar to the Magellanic fauna by the addition of cold-temperate taxa [13].

Unfortunately, the Neogene record of seabirds in other marine formations of the Southeast Pacific is comparatively scarce and consequently poorly known [14–18]. Most of these records are Pliocene in age, being younger than the main assemblages recorded in Bahia Inglesa and Pisco, and giving us an exceptional opportunity for the study of changes in the composition of seabird faunas over time. However, all these localities are restricted to the PCP in Northern Chile and Southern Peru. In consequence, our knowledge of the evolutionary history of seabirds in the transitional zone during the Neogene is negligible.

In this context, the discovery of a new assemblage of fossil birds in the coastal locality of Horcon in central Chile offers a unique

opportunity to fill this gap for southern temperate areas and, along with the previously known Pliocene records, reveals changes in the composition of seabird faunas in the area of influence of the Humboldt Current during the last 5 Ma.

Materials and Methods

The Horcon Formation

The specimens described here come from coastal outcrops of the Horcon Formation [19,20], located 51 km north to the city of Valparaiso between the villages Horcon and Maitencillo in the Valparaiso Region, central Chile (see Figure S1.1 in Document S1).

The lithology of the Horcon Formation is characterized by predominance of subhorizontal, unconsolidated fine sandstones with a dip of 2° to 3°. The estimated thickness of the sequence is 45 m and two well-defined stratigraphic intervals can be identified. All the specimens described here come from the upper unit, which corresponds to the main section of the sequence (see Figure S1.2 in Document S1). This unit is characterized by layers of fine to coarse sandstone, light-colored and poorly consolidated, which are interspersed with few conglomeritic layers. Vertebrate and invertebrate macrofossils are abundant in all the sandstone strata, with over 60 taxa recognized so far, making the Horcon Formation one of the most diverse and the southernmost marine vertebrate assemblages currently known for the Neogene in the Southeastern Pacific [21]. The stratigraphic column for this formation can be found in Document S1.

Tavera [20] assigned the Horcon Formation to the Pliocene based on the mollusk biostratigraphy. The new mollusk specimens collected during this study, which include the bivalves *Chlamys* cf. *hupeanus* and *Panopea coquimbensis* along with the gastropods *Chorus blainvillei*, *Chorus doliaris* and *Herminespina mirabilis*, corroborate an age not younger than Late Pliocene [22–28].

Repository information

The material consists of eighteen specimens including a set of associated wings and pectoral girdle elements (SGO-PV 21443) deposited in the Vertebrate Palaeontological collection of the Museo Nacional de Historia Natural, Santiago (Chile), under accession numbers SGO-PV 21443 to 21455 and SGO-PV 21487 to 21490. All necessary permits were obtained for the described study, which complied with all relevant regulations. The collection of these specimens was authorized by the Consejo de Monumentos Nacionales (Chile) through the order number 4703, enacted on September 24th, 2010.

Nomenclatural Acts

The electronic edition of this article conforms to the requirements of the amended International Code of Zoological Nomenclature, and hence the new names contained herein are available under that Code from the electronic edition of this article. This published work and the nomenclatural acts it contains have been registered in ZooBank, the online registration system for the ICZN. The ZooBank LSIDs (Life Science Identifiers) can be resolved and the associated information viewed through any standard web browser by appending the LSID to the prefix "http://zoobank.org/". The LSID for this publication is: urn:lsid:zoobank.org:pub: 5DE13597-E734-453B-8703-F42F84f-206A38. The electronic edition of this work was published in a journal with an ISSN, and has been archived and is available from the following digital repositories: PubMed Central, LOCKSS.

Phylogenetic analysis

To explore the phylogenetic relationship of the new penguin species described here (Figure 1), we expanded and modified a recently published combined matrix [29], including 246 morphological characters plus five genes (RAG-1, 12S, 16S, COI, and cytochrome b) with over 6000 basepairs. We added eight new osteological characters for the humerus and tarsometatarsus, new states for five of the previously used characters and a modification of the definition of two other characters. The list of characters, detail of the modifications to the original matrix and the GenBank accession numbers are provided in Document S1; and a nexus file of the entire data set is provided as Dataset S1.

Three of the taxa previously included by Ksepka *et al.* [29] were identified as wildcards, labile taxa that reduce the resolution of the consensus tree, and excluded from the final analysis: *Delphinornis wimani*, *Palaeeudyptes antarcticus* and *Duntroonornis parvus*. From the taxa added by Ksepka and Thomas [30], only *Inguza predemersus* was included in the final analysis; *Nucleornis* was included during preliminary analysis, but was identified as a wildcard and excluded from the final analysis. As a result, the current analysis includes 55 penguin taxa. All South American taxa included here were coded by direct observation, with the only exception of "*Pygoscelis*" *grandis*. The outgroup includes 13 species of Procellariiformes and two species of Gaviiformes. The trees were rooted on Gaviiformes.

The phylogenetic analysis was conducted following the strategy defined by Ksepka *et al.* [29], using PAUP4.0b10 [31] with a heuristic search strategy (1000 replicates of random taxon addition saving 10 trees per replicate, with TBR branch swapping). All characters were equally weighted, multistate coding was used only to represent polymorphism, and branches with a minimum length of zero were collapsed. A morphology-only and morphology plus molecular data analysis were done. Strict and Adams consensus trees were calculated for each analysis, but only the strict consensus are presented, showing the best-solved topology. Additional consensus trees can be found in the Figure S3 in Document S1.

Results

Systematic palaeontology

Sphenisciformes Sharpe, 1891.

Spheniscidae Bonaparte, 1831.

Eudyptes Vieillot, 1816.

Eudyptes calauina sp. nov.

(Figures 1A–I, L–W, 2, Figure S2A–B in Document S1)

ZooBank life science identifer (LSID) for species. urn:lsid:zoobank.org:act: ECFC692D-4AA8-4AE6-8B56-307B416A432F

Etymology. Noun in apposition. Calauina (kalɣɛnɑ) is the name of the rockhopper penguin (*Eudyptes chrysocome*) in the quasi-extinct Yaghan language, spoken by the Yagán people from Tierra del Fuego, Southern Chile.

Holotype. SGO-PV 21487, complete right tarsometatarsus (Figure 1L–Q, Figure S2A in Document S1).

Paratype. SGO-PV 21444, complete right tarsometatarsus (Figure 1R–W, Figure S2B in Document S1).

Referred materials. SGO-PV 21452, cervical vertebrae; SGO-PV 21451, left humerus lacking humeral head (Figure 1B–D); SGO-PV 21448, distal portion of left humerus; SGO-PV 21449, proximal fragment of left humerus (Figure 1E–G); SGO-PV 21447, proximal portion of right tibiotarsus (Figure 1H); SGO-PV 21488, distal portion of right tibiotarsus (Figure 1I); SGO-PV 21445, pedal phalanx; SGO-PV 21453, fragment of pedal phalanx.

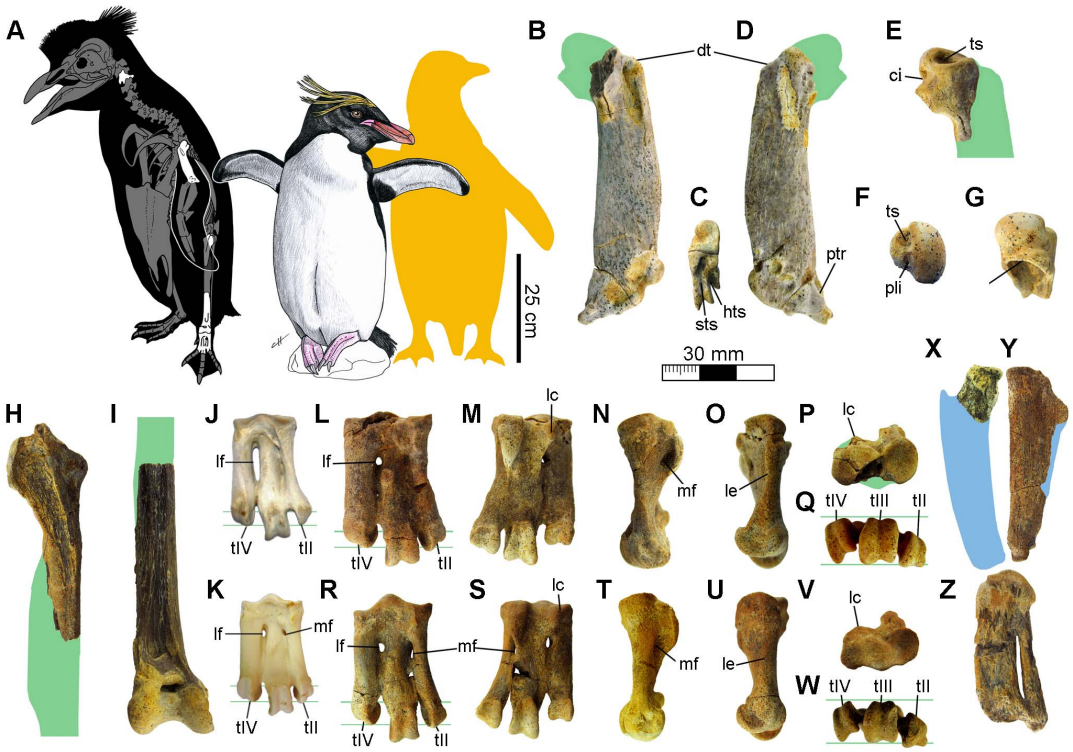

Figure 1. Fossil penguins from the Horcon Formation. A. Skeletal reconstruction of *Eudyptes calauina* sp. nov. showing the identified elements; and size comparison with the Macaroni penguin *E. chrysolophus* and the Yellow-eyed penguin *Megadyptes antipodes* (yellow silhouette). Referred specimens: left humerus (SGO-PV 21451) in (**B**) cranial, (**C**) distal and (**D**) caudal views; proximal fragment of left humerus (SGO-PV 21449) in (**E**) cranial, (**F**) proximal and (**G**) ventral views; (**H**) proximal fragment of right tibiotarsus (SGO-PV 21447) in cranial view; and (**I**) distal portion of right tibiotarsus (SGO-PV 21488) in cranial view. Tarsometatarsus of Humboldt penguin *Spheniscus humboldti* (**J**) and Northern Rockhopper penguin *E. moseleyi* (**K**). Holotype: right tarsometatarsus attributed to an adult (SGO-PV 21487) in (**L**) dorsal, (**M**) plantar, (**N**) medial, (**O**) lateral, (**P**) proximal and (**Q**) distal views. Paratype: right tarsometatarsus attributed to a subadult (SGO-PV 21444) in (**R**) dorsal, (**S**) plantar, (**T**) medial, (**U**) lateral, (**V**) proximal and (**W**) distal views. Spheniscidae indet.: (**X**) proximal fragment of right radius (SGO-PV 21450) in ventral view; (**Y**) right ulna (SGO-PV 21455) in ventral view; and (**Z**) right carpometacarpus (SGO-PV 21454) in ventral view. Silhouettes (green for *E. calauina*, blue for Spheniscidae indet.) based on complementary specimens attributed to the same species or living relatives. **Abbreviations:** ci, capital incisure; dt, dorsal tubercle; hts, humerotricipital sulcus; lc, lateral hypotarsal crest; le, lateral edge of the metatarsi IV; lf, lateral proximal vascular foramen; mf, medial proximal vascular foramen; pli, pit for ligament insertion; ptr, posterior trochlear ridge; sts, scapulotricipital sulcus; tf, tricipital fossa; tII, trochlea metatarsi II; tIII, trochlea metatarsi III; tIV, trochlea metatarsi IV; ts, transverse sulcus.
doi:10.1371/journal.pone.0090043.g001

Type locality and horizon. Horcon Formation, Late Pliocene, Chile. SGO-PV 21487, 21452, 21448, 21449, 21488 and 21453 collected from layer 12 (Figure S1.2 in Document S1). SGO-PV 21444 collected from layer 8. SGO-PV 21451 collected from layer 9. SGO-PV 21445 collected from layer 10.

Diagnosis. Larger than *Megadyptes antipodes*, *Spheniscus chilensis* and *S. humboldti*; but smaller than *S. urbinai* and *Pygoscelis grandis*. The tarsometatarsus is on average 30% larger than *Eudyptes sclateri*, 16% larger than *Megadyptes antipodes* and 12% larger than *Madrynornis*. Based on the humerus, *E. calauina* can be differentiated from other species of the genus by (i) the presence of a slightly concave and asymmetrical proximal border of the tricipital fossa in ventral view instead of the stronger symmetrical concavity common in extant species, (ii) a more robust humeral shaft with a robustness index (proximodistal length/ventrodorsal width at middle point) of 4 whereas in extant species it is between 4.5 and 4.9 (see Character 176 in Document S1), and (iii) a scapulotricipital sulcus separated from the humerotricipital sulcus and not dorsally connected as in other species. At the level of the tarsometatarsus, it can be differentiated by (i) an elongation index between 1.7 and 1.8 (Figure 2), (ii) a moderately deep medial dorsal sulcus instead of the occasionally shallow one observed in other species, (iii) a strongly dorsoplantarly compressed lateral edge of metatarsus IV creating a sharp edge in lateral view, unlike the wider and rounded edge in extant species, and (iv) a slightly pointed trochlea II with parallel medial and lateral edges in plantar view, instead of the strongly pointed one with a more rounded medial edge of extant species. An expanded description of the specimens assigned to *E. calauina* is provided in Document S1.

Measurements. SGO-PV 21487: length at middle point 41.3 mm; proximal mediolateral width 24.3 mm; distal mediolateral width 27.5 mm. SGO-PV 21444: length at middle point 41 mm; proximal mediolateral width 22.7 mm; distal mediolateral width 25.3 mm. SGO-PV 21451: maximum preserved length 76.8 mm; diaphysis length 69.4 mm; ventrodorsal width at middle point 17.4 mm. A comparative table of measurements for the tarsometatarsus is provided in Table S1 in Document S1.

Anatomical remarks

Although all specimens have been found isolated, all of them are similar in morphology to homologous elements of the genus *Eudyptes* and larger than in *Megadyptes*. The most diagnostic elements of this set are the tarsometatarsus (SGO-PV 21487 and SGO-PV 21444) and humerus (SGO-PV 21451 and SGO-PV

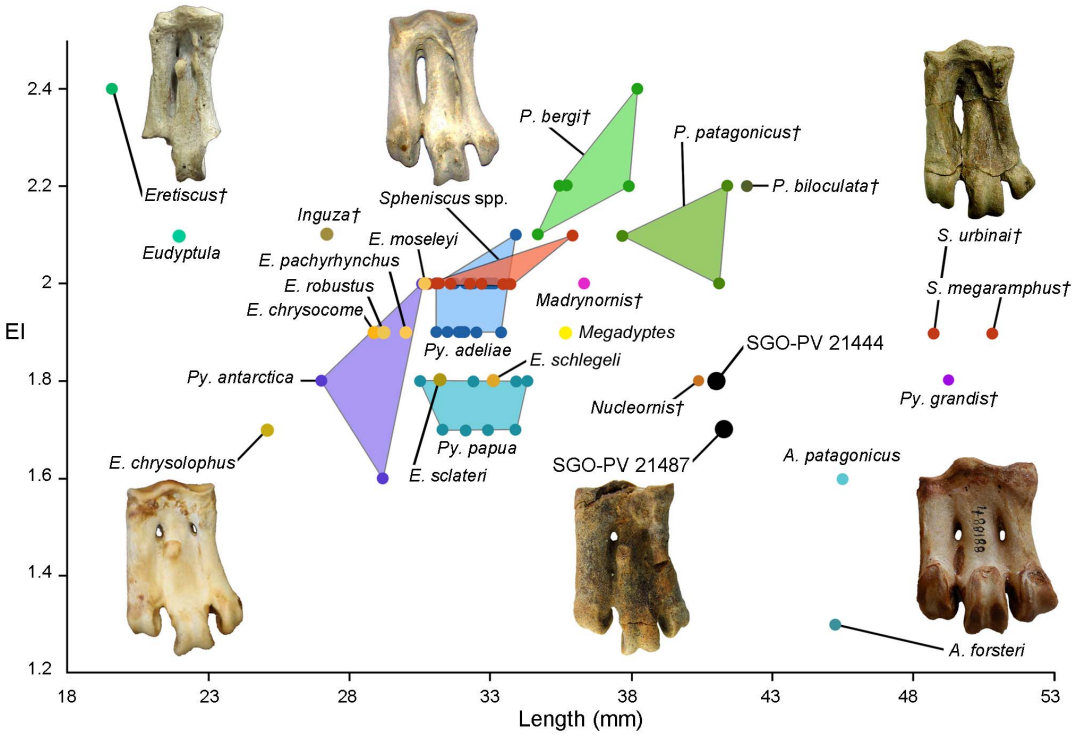

Figure 2. Tarsometatarsus elongation index vs length. Plot of the tarsometatarsus elongation index (EI, obtained from the division of the proximodistal length per the mediolateral width at the proximal end) against the proximodistal length of tarsometatarsus in Neogene penguins.
doi:10.1371/journal.pone.0090043.g002

21449); both elements widely used for the typification of fossil penguins and showing the same distinctive combination of characters as in *Eudyptes*, whereas all the other specimens are referred mainly based on their size range and general morphology. Consequently, only the tarsometatarsus and humerus are used for the diagnosis.

This new species can be assigned to the genus *Eudyptes* based on a combination of 23 osteological characters. Of these, ten allow us to discriminate this species from *Spheniscus* (Figure 1J), the only penguin genus that currently inhabits the area and the most common one in the fossil record of Chile and Peru. These characters are, at level of humerus: (i) humeral head strongly prominent proximally (slightly prominent in *Eudyptula* and *Spheniscus*); (ii) notch between dorsal tubercle and humeral head present (usually absent in *Spheniscus*, *Eudyptula* and *Tereingaornis*); (iii) capital incisure completely separated from transverse ligament sulcus (connected through narrow sulcus in *Aptenodytes*, *Inguza*, *Madrynornis*, *Palaeospheniscus* and *Eretiscus*); (iv) presence of deep pit for ligament insertion adjacent to head on proximal surface (absent or very shallow in *Pygoscelis antarctica*, *P. adeliae*, *Madrynornis*, *Palaeospheniscus*, *Eretiscus* and occasionally in *Aptenodytes patagonicus*); (v) proximal margin of tricipital fossa weakly projected in proximal view (well-exposed in extant species of *Spheniscus* and occasionally in *Pygoscelis antarctica*); (vi) impressio insertii m. supracoracoideus and m. latissimus dorsi separated by small gap (separated by moderate gap in *Palaeospheniscus*, *Eretiscus* and occasionally in *Spheniscus urbinai*); (vii) shaft robustness index between 4 and 5 (between 5 and 6 in *Eudyptula*, *Inguza*, *Madrynornis* and *Eretiscus*); (viii) nutrient foramen situated on ventral face of shaft (situated on anterior face in *Madrynornis* and *Eretiscus*); (ix) preaxial angle weak or absent (well defined in *Aptenodytes*, *Pygoscelis*, *Megadyptes*, *Spheniscus*, *Palaeospheniscus*, *Eretiscus* and occasionally in *Eudyptes*); (x) posterior trochlear ridge reaching ventral edge of the shaft (extends beyond ventral margin in *Aptenodytes*, *Pygoscelis* and *Madrynornis*; but does not reach ventral edge in *Inguza*, *Eretiscus* and some species of *Spheniscus*); (xi) trochlear angle greater than or equal to 45° (between 35° and 45° in *Inguza*, *Madrynornis*, *Tereingaornis* and occasionally slightly under 45° in *Spheniscus urbinai*, *Palaeospheniscus* and *Eretiscus*); and (xii) ulnar condyle almost parallel to radial and not surpassing anterior edge of humerus (slightly surpassing anterior edge in *Madrynornis*, *Palaeospheniscus* and *Eretiscus*).

At level of tarsometatarsus: (xiii) elongation index less than 2 (between 2 and 2.5 in extant species of *Spheniscus*, *S. muizoni*, *Megadyptes*, *Eudyptula*, *Inguza*, *Madrynornis*, *Palaeospheniscus*, *Eretiscus* and occasionally in *Pygoscelis adeliae* and *Eudyptes moseleyi*); (xiv) inconspicuous colateral lateral ligament scar (creating depression over lateral surface in *Pygoscelis*; and creating notch on proximo-lateral vertex in *Spheniscus*, *Eudyptula*, *Inguza*, *Nucleornis*, *Madrynornis*, *Palaeospheniscus* and *Eretiscus*); (xv) medial hypotarsal crest projected farther than lateral crest (both reach same projection in *Pygoscelis*); (xvi) intermediate hypotarsal crest indistinguishable from lateral crest (slightly separated by shallow groove in proximal view in *Madrynornis*, *Palaeospheniscus*, *Eretiscus* and occasionally in *Eudyptula* and *Eudyptes chrysocome*); (xvii) lateral hypotarsal crest forming diagonal ridge that overhangs lateral foramen (poorly defined and proximal to lateral foramen in *Aptenodytes*, *Pygoscelis*, *Megadyptes*, *Eudyptula*, *Spheniscus* and *Nucleornis*), (xviii) large medial proximal vascular foramen opening plantarly at medial surface of medial hypotarsal crest (often smaller in *Spheniscus* and *Eudyptula*; opening at plantar surface in *Aptenodytes*, *Pygoscelis* and *Nucleornis*; vestigial in *Palaeospheniscus* and *Eretiscus*); (xix) small lateral proximal vascular foramen (occasionally enlarged in *Spheniscus*; vestigial in *Eretiscus*; and absent in *Nucleornis*); (xx) lateral intertrochlear notch deeper than medial (sub-equal to equal in *Aptenodytes*, *Pygoscelis*, *Megadyptes*, *Spheniscus urbinai*, *S. megaramphus* and *Inguza*); (xxi) trochlea metatarsi

IV shorter than II in dorsal view (sub-equal to equal in *Aptenodytes*, *Pygoscelis*, *Megadyptes*, *Eudyptula* and *Spheniscus*); (xxii) trochlea metatarsi III and IV aligned at the same plane in distal view (trochlea IV displaced dorsally in extant species of *Spheniscus* and *S. megaramphus*); and (xxiii) trochlea metatarsi II slightly deflected plantarly in distal view (strongly deflected in *Eudyptula*, *Spheniscus megaramphus* and *Palaeospheniscus*).

The tarsometatarsus SGO-PV 21487 (Figure 1L–Q) is 16% larger than in *Megadyptes*; whereas the best-preserved humerus available SGO-PV 21451 (Figure 1B–D) is approximately 5% larger than in *Megadyptes*. The elongation index (EI), obtained from the division of the proximodistal length per the mediolateral width at the proximal end of the tarsometatarsus, is 1.7 for SGO-PV 21487 and 1.8 for SGO-PV 21444 being within the range of *Eudyptes chrysolophus* (1.7), *E. sclateri* (1.8), *E. schlegeli* (1.8), *Pygoscelis papua* (1.7–1.8), *P. antarctica* (1.6–2.0), *P. grandis* (1.8) and *Nucleornis* (1.8). This is smaller than in *E. moseleyi*, *E. chrysocome*, *E. pachyrhynchus* and *E. robustus*. In a plot of the EI against the proximodistal length (Figure 2), it is evident that both specimens are separated from South American extant and fossil penguins; with *Nucleornis* from the Early Pliocene of South Africa being the only similar taxon in size and proportions. However, the EI of *Nucleornis* is based on an approximation of the proximal width and the morphology of this element is clearly distinguishable from *E. calauina*.

Ontogenetic stages of specimens

Taking as reference the extant species of *Eudyptes* and *Megadyptes*, where the average length of the tarsometatarsus is approximately 45% of the length of the humerus, SGO-PV 21451 is approximately 13% smaller than the size expected based on the holotype (91.7 mm). We estimate the expected size range for the humerus, calculated as the linear measure $+/-1.96$ per the standard deviation [32], using the standard deviation for the humerus length in *E. pachyrhynchus* (2.1) [33]. The expected size range is between 87.6 and 95.8 mm, suggesting that SGO-PV 21451 is approximately 10% smaller than expected based on the proportions of living species of *Eudyptes*. Considering the relatively smooth surface texture of the humerus SGO-PV 21451, along with the well-defined edges and muscular attachments, this specimen can be attributed to an adult or late subadult [34]. In consequence, the difference in proportion observed cannot be easily attributed to the aging of the individuals. This can be an indication of a slightly different humerus-tarsometatarsus proportion in *E. calauina* as has been described in fossil species of *Spheniscus* [35]. There is evidence of variation in the average proportion represented by the tarsometatarsus among *Eudyptes* species: 45.8% in *E. chrysocome*, 45.4% in *E. pachyrhynchus*, 45.3% in *E. robustus* and 42% in *E. sclateri*. Considering a reconstructed length of 80 mm for the humerus SGO-PV 21451, and assuming that it belongs to the same individual as the holotype, the proportion in *E. calauina* will be close to 50%; being 5% higher than in most of the living species. This is similar to the proportion in *Eudyptula* (50%) and similar to the range of difference between *Aptenodytes patagonicus* (40.2%) and *A. forsteri* (34%). Nevertheless, it is clear that both elements belong to different individuals and the lack of associated elements does not allow a more detailed comparison.

On the other hand, it is important to note that whereas the holotype SGO-PV 21487 can be attributed to an adult (Figure 1L–Q), the paratype SGO-PV 21444 most likely represents a subadult individual (Figure 1R–W). This is based on the slight size difference, the more porous texture of the bone (Figure S2.A–B in Document S1) and the degree of development of some anatomical features in SGO-PV 21444, like the larger medial foramen and the deeper and more angular intertrochlear notches. For this reason, the diagnosis for the tarsometatarsus is based mostly on the holotype. Nevertheless, both specimens share the most diagnostic characters of the genus.

Phylogenetic analysis

Analysis of the combined data set resulted in 192 most parsimonious trees (MPTs) of 5563 steps (Figures 3A, Figure S3.1-2 in Document S1), whereas the morphology-only analysis resulted in 704 MPTs of 802 steps (Figure 3B, Figure S3.3-4 in Document S1). Both analyses recovered fewer trees than Ksepka *et al.* [29], a difference attributed primarily to the exclusion of the wildcard taxa and a more complete data set. Our results also show better resolution and recover all the genera as monophyletic, with the exception of *Archaeospheniscus* and *Pygoscelis*. Topologies of the combined and morphology-only strict consensus trees are almost identical for the stem penguin taxa, but there is disagreement in the topology of the crown group between both analyses (Figure 3).

The general relations among the stem genera are similar to those previously reported [29,30]; however, a new series of pairings has been obtained. *Mesetaornis* and *Marambiornis* are joined close to the base of the Spheniscidae. The large polytomy recovered by Ksepka *et al.* [29], including *Palaeeudyptes*, *Inkayacu*, *Icadyptes* and *Pachydyptes* is better resolved. The two Antarctic species attributed to *Palaeeudyptes*, *P. gunnari* and *P. klekowskii*, are now separated from this polytomy as a more basal node. Three clades, composed of *Inkayacu*+the Burnside "*Palaeeudyptes*", *Kairuku waitaki*+*Kairuku grebneffi* and *Icadyptes*+*Pachydyptes* are also recovered. They appear in a polytomy in both strict consensus trees (Figure 3). Additionally, *Palaeospheniscus* is recovered as monophyletic with respect to *Eretiscus*. A list of the osteological synapomorphies that support these clades and the monophyly of the extant genera can be found in Document S1.

Our results show a better-resolved topology for the crown group than previous analyses at level of genera [29,30]. All the fossil taxa recovered as part of the crown group, with the possible exception of *Inguza*, are from the Neogene of South America. The strict consensus of our combined analysis shows *Madrynornis* and *Inguza* in an unsolved relationship with the clade containing the Antarctic penguins (*Aptenodytes*+*Pygoscelis*) and the temperate-tropical group containing the remaining extant genera (Figure 3A); whereas the morphological analysis joins both genera as the sister group of the crown Spheniscidae (Figure 3B). These taxa are also recovered outside Spheniscidae in the Adams consensus of the combined analysis (Figure S3.2 in Document S1). *Madrynornis* from the Middle Miocene of Argentina had been previously recovered as sister of *Eudyptes* within Spheniscidae [30,36]; while in the case of *Inguza* from the Early Pliocene of South Africa, a closer relationship with the temperate-tropical group had been previously suggested [30]. This change is mainly the result of the modification of some characters and the substantial decrease in the percentage of missing-data for *Madrynornis*, which is reduced from 47.7 to 15.5 for osteological characters. In contrast with the most recent analyses [29,30], the inclusion of both taxa within Spheniscidae slightly reduces the resolution of the strict consensus of the combined analysis in comparison with the morphology-only analysis. This decrease in resolution can be linked to a general problem regarding osteological characters: the high intrageneric homogeneity and intraspecific variation observed among extant taxa. In consequence, some of these characters must be coded as polymorphic, reducing their strength in comparison with the molecular data and collapsing some nodes in the combined analysis. It is expected that the addition of new characters and the reduction of missing data for fossil taxa will improve the resolution

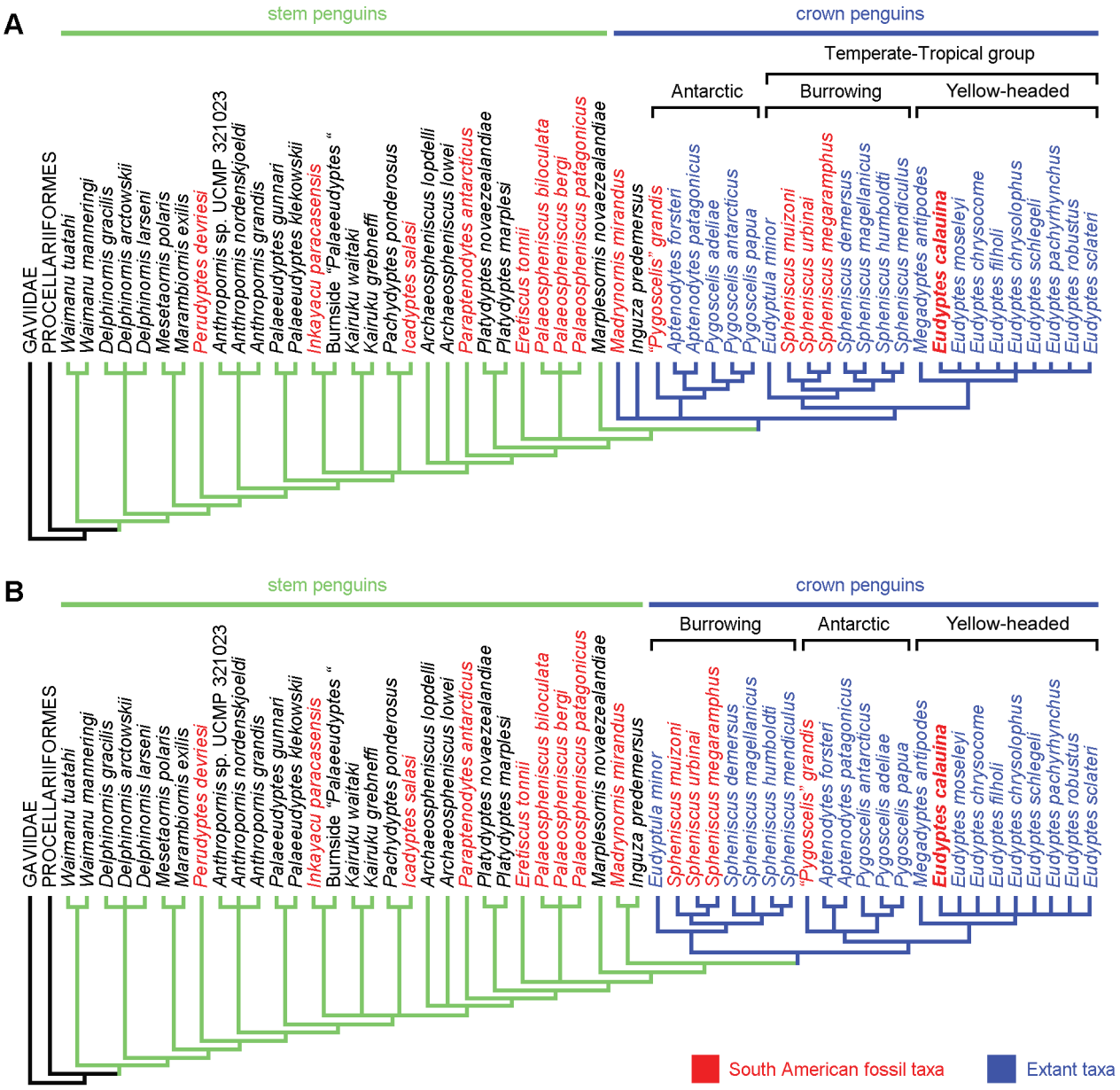

Figure 3. Phylogenetic relations of *Eudyptes calauina* sp. nov. A. Strict consensus tree of 192 MPTs (tree length = 5563 steps, rescalated consistency index [RC] = 0.373, retention index [RI] = 0.699) from a combined analysis of morphological characters plus >6000 bp. **B.** Strict consensus tree of 704 MPTs (tree length = 802 steps, RC = 0.492, RI = 0.879) from an analysis of morphological-only characters.
doi:10.1371/journal.pone.0090043.g003

of the analyses as will improving completeness of molecular data for extant taxa.

All our analyses recover three main clades within Spheniscidae: (i) the Antarctic penguins, (ii) the burrowing penguins, and (iii) the yellow-headed penguins (Figure 2). The first one includes the truly Antarctic penguins joining the great penguins (*Aptenodytes*) and brush-tailed penguins (*Pygoscelis*). This clade has been previously recovered by morphology-only analyses [37,38] and more recently by a molecular analysis [39], but both genera are always recovered in separate basal nodes in most molecular [40] and combined analyses [29,30,41]. In our results, the Antarctic group also includes the fossil species "*Pygoscelis*" *grandis* joined in a basal node. "*Pygoscelis*" *grandis* was originally included as a stem taxon of *Pygoscelis* [37], but subsequent analyses recovered it in different positions within the crown group [29,41]. Unfortunately, the character states for this taxon have been taken from the literature in the latest analyses, so that a direct revision of the type specimen is required to resolve their affinities.

The burrowing penguins include the blue penguin (*Eudyptula*) and the banded penguins (*Spheniscus*), and had been recovered as a monophyletic group by molecular, morphological, and combined analysis [29,39,40,41]. Within the banded penguins, a dichotomy between the extant species and the South American fossils is always recovered in our analysis. This differs from the relations presented by previous studies [29], in which *S. muizoni* is more closely related to the crown *Spheniscus* than to *S. urbinai* and *S. megaramphus*. This change is mainly due to the increase in the number of characters coded for the South American fossils.

Finally, the yellow-eyed penguin (*Megadyptes*) plus the crested penguins (*Eudyptes*) form the yellow-headed penguins clade, well supported by molecular, morphological, and combined analysis [29,39,40,41]. *Eudyptes calauina* is always recovered within the crested penguins in our analysis. Despite the lack of internal resolution in the strict consensus (Figure 3), the crested penguins are always recovered as a monophyletic clade with the yellow-eyed penguin as sister taxon. The lack of internal structure in the strict consensus within *Eudyptes* is most likely related to the high percentage of missing molecular data, which in some species exceeds 80%. Nevertheless, part of the internal topology is recovered by the Adams consensus (Figure S3.2, S3.4 in Document S1)

The main difference between the combined and morphology-only analysis is the relationship between these three main clades derived from the rooting [42]. A temperate-tropical group (clade A in [30]) containing the burrowing and yellow-headed penguins has always been recovered as monophyletic in molecular [39,40] and combined analyses [29,30,41] (Figure 3A), and the Adam consensus of our combined analysis recovers a dichotomy between the Antarctic penguins and the temperate-tropical penguins (Figure S3.2 in Document S1). On the other hand, morphology-only analyses often recover the burrowing penguins as the most basal node within Spheniscidae, joining the Antarctic and yellow-headed penguins in a more derived clade [37,38,41] (Figure 3B). This topology is collapsed in some of the most recent morphological trees [29,30], most likely due to the inclusion of wildcard taxa. It is important to mention, that this does not affect the placement of *Eudyptes calauina* within the crested penguins; and despite these differences, the main relations between genera are largely congruent. It has been suggested that the study of fossil taxa representing the proximal outgroups to the crown Spheniscidae could help to improve its rooting [42]. In this sense, our results suggest that the study of the relationships of *Madrynornis* and *Inguza* can be key to improve the congruence between molecular and morphological data.

Spheniscidae indet

Referred materials. SGO-PV 21489, fragment of right coracoid; SGO-PV 21450, proximal fragment of right radius (Figure 1X); SGO-PV 21455, right ulna (Figure 1Y); SGO-PV 21454, right carpometacarpus (Figure 1Z); SGO-PV 21457, distal fragment of left carpometacarpus. All specimens collected from layer 12. Measurements in table 1.

Remarks

All the specimens included here are morphologically similar to *Spheniscus* and *Eudyptes* and in the size range of *Spheniscus humboldti* and *S. chilensis*, being approximately 20% smaller than the size expected for *E. calauina*. These may represent a second and smaller species of penguin or juveniles of *E. calauina*.

The fibrous textures observed in the ulna SGO-PV 21455 (Figure 1Y, Figure S2.C in Document S1) and the carpometacarpus SGO-PV 21454 (Figure 1Z) allow us to attribute these specimens to immature individuals. Based on the proportions of the flipper elements in *Eudyptes*, *Spheniscus* and *Megadyptes* [43], and the length of the carpometacarpus SGO-PV 21454, we calculate the expected length for the main elements of the appendicular skeleton (Table 1). The recorded length of the ulna SGO-PV 21455 is congruent with the expected size. However, the humerus SGO-PV 21451 is approximately 12% larger than the expected length based on the carpometacarpus. These differences suggest that both specimens belong to two separate taxa or, as the surface texture suggests, to different ontogenetic stages, whereas the ulna and carpometacarpus possibly belong to the same taxon and a similar ontogenetic stage. Unfortunately, the fragmentary nature of these specimens and the fact that at least some of them belong to immature individuals, make it impossible to offer a more specific assignation.

Procellariiformes Fürbringer, 1888.

Procellariidae Leach, 1820.

Puffinus Brisson, 1760.

Puffinus cf. *griseus* Gmelin, 1789.

Referred materials. SGO-PV 21490, proximal fragment of left tarsometatarsus (Figure 4A,C,E,F). Collected from layer 12.

Measurements. Maximum length preserved, 43.8 mm; proximal mediolateral width, 9.7 mm; dorsoplantar width of shaft at the middle point, 4.29 mm.

Anatomical comparison

In dorsal view, the medial cotyla is medially expanded, giving an asymmetric appearance to the proximal end of the tarsometatarsus as in *P. griseus*, *P. gravis* and *P. bulleri*, but weaker than in *P. pacificus*. In genera such as *Calonectris*, *Pterodroma* and *Pterodromoides* the proximal end is more symmetrical. The medial cotyla is also located more proximally than the lateral cotyla as is usual in *Puffinus*, whereas in *Calonectris* both cotylae are of subequal height. The medial margin of the medial cotyla is strongly pointed as in *Puffinus* and *Calonectris*. The intercotylar prominence is slightly damaged and is relatively wide as in *P. griseus* and *P. bulleri*, being smaller that in *P. gravis* and *P. creatopus* and less rounded that in *P. pacificus*. As in *P. griseus*, *P. gravis* and *P. pacificus* the dorsal infracotylar fossa is completely open, whereas in *P. creatopus*, *Calonectris* and *Bulweria* the retinacular extensors scar (impressio retinacula extensorii) forms a bridge that covers the medial foramen. In *P. bulleri* the retinacular extensors scar forms a smaller ridge proximal to the medial foramen.

The hypotarsal crests are partially preserved. In proximal view, well-defined lateral and medial canals can be identified. The presence of both canals is typical of *Puffinus*, whereas a lateral canal partially close and a medial sulcus can be seen in genera like *Pterodroma* and two shallow sulci are present in *Fulmarus*.

The middle shaft is strongly mediolaterally compressed as in *Puffinus*, whereas in genera like *Calonectris*, *Bulweria*, *Pterodroma*, *Pterodromoides* and *Pachyptyla* the shaft is more expanded mediolaterally. From the middle point of the shaft to the proximal end, the shaft gradually expands mediolaterally as in *P. griseus*, *P. creatopus* and *P. bulleri*; whereas in *P. gravis*, *P. pacificus* and *Calonectris* the width of the shaft is more constant, expanding proximally only at the level of the proximal foramina. The dorsal sulcus is shallow and poorly defined as in *Puffinus*, whereas in genera like *Pterodroma* and *Pterodromoides* it is deep and well delimited by medial and lateral ridges.

Remarks

This specimen is equivalent in size and morphology to the extant *Puffinus griseus*, one of the largest shearwaters and a much larger taxon than most of the fossils previously attributed to *Puffinus* in the Southeastern Pacific [44]. It represents a species smaller than *P. gravis* and *Procellaria*, similar in size to *Calonectris* and larger than *Puffinus creatopus*, *P. bulleri* and *P. pacificus*. Nevertheless, considering the fragmentary nature of this record and the intraspecific and interspecific variation within the extant species [44], we avoid a more specific assignment.

All the specimens described by Stucchi and Urbina [44], from the Miocene of the Pisco Formation represent species similar in size or smaller than *P. bulleri* and *P. pacificus*. Additionally, an isolated neurocranium from the Late Miocene of the Bahia Inglesa

Table 1. Length measured and expected for flipper element.

	Measured	Specimen measured	Expected	Percentage of total length
Humerus	76.8[a] (80[b])	SGO-PV 21451	70.1+/−4.5	33%
Ulna	53.1	SGO-PV 21455	51	24%
Carpometacarpus	42.5	SGO-PV 21454	42.5	20%

The expected lengths were calculated base on the proportions described for *Eudyptes*, *Spheniscus* and *Megadyptes* [42], and using the carpometacarpus SGO-PV 21454 as reference specimen. The range for the humerus was calculated based in the method of Warheit [32] (measure +/− 1.96 x standard deviation) and using the standard deviation offered by Livezey [42] for the humerus of *Spheniscus magellanicus* (2.3). Note that the humerus SGO-PV 21451 is larger than the expected length.
[a]. Maximum conserved length,
[b]. Estimated total length.
doi:10.1371/journal.pone.0090043.t001

Formation has been attributed to *Puffinus* [45], and represents a shearwater larger than *P. griseus* and *P. creatopus*. This specimen possibly belongs to the same taxon as the skull found in the Pisco Formation and erroneously attributed to *Fulmarus* by Cheneval [5]. Other Pliocene records of *Puffinus* in the Eastern Pacific include the extinct Early Pliocene species *P. tedfordi* [46] from Baja California, Mexico, and *P. fethami* [47] from California, USA; and the Late Pliocene *P. kanakoffi* [47] and *P. gilmorei* [48] from San Diego, USA. All these species are smaller than *P. griseus*.

Suliformes (Sharpe, 1891).

Phalacrocoracidae Reichenbach, 1850.

Phalacrocorax Brisson, 1760.

Phalacrocorax sp.

Referred materials. SGO-PV 21443, associated wings and pectoral girdle elements including left and right coracoids, proximal fragment of right scapula, proximal fragment of right humerus, right ulna lacking of proximal end, right radius lacking of proximal end, distal fragment of left ulna, proximal fragment of right carpometacarpus (Figure 4H–O); SGO-PV 21446, proximal fragment of left carpometacarpus. SGO-PV 21443 collected from layer 12; SGO-PV 21446 collected from layer 9.

Measurements. SGO-PV 21443, left coracoid, maximum length preserved 53.6 mm; left coracoid, sternal facet width 16.4 mm; right coracoid, maximum length preserved 57.1 mm; right scapula, proximal width 14.2 mm; right humerus, maximum proximal width 20.1 mm; right ulna, maximum length preserved 103.8 mm; right carpometacarpus, proximal anteroposterior width 12 mm.

Remarks

These specimens represent a cormorant smaller than *Phalacrocorax bougainvilli* and similar in size to *P. gaimardi* and *P. brasilianus*. This range is equivalent to that described for *Phalacrocorax* sp. from the Late Miocene and Pliocene of the Pisco Formation [5,7], and the Late Pliocene of the La Portada Formation [16]. Similar specimens are also known from the Late Miocene of the Bahia Inglesa Formation, including an associated braincase and sternum [18,49]. A second and larger species, *P.* aff. *bougainvillii*, is also known from the Late Miocene and Pliocene of the Pisco and Bahia Inglesa formations [2,7,18].

As has been mentioned by previous authors [7] and based on the differences in the proportions respective to extant Pacific cormorants, these specimens probably represent an extinct species. Despite the fact that SGO-PV 21443 is one of the most complete specimens of seabird currently known from Chile, here we avoid naming a new species, considering the availability of more

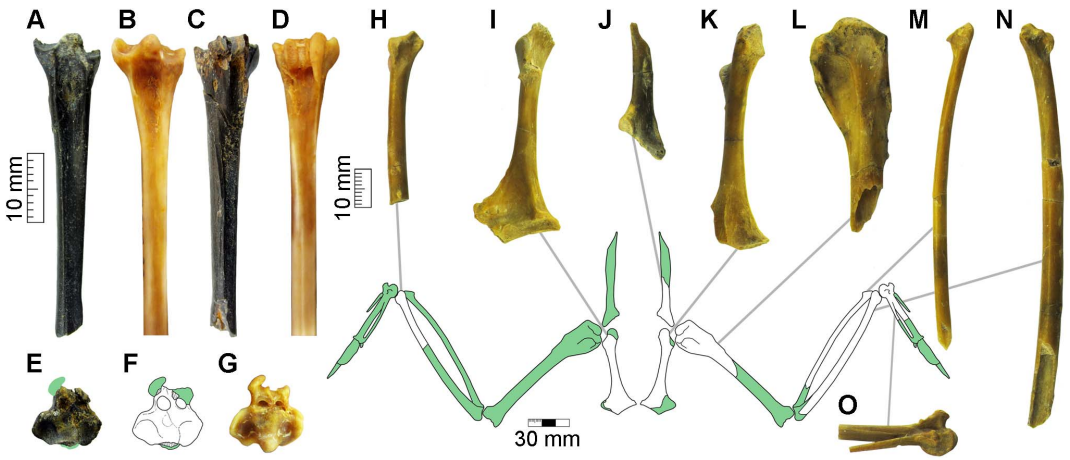

Figure 4. Fossil shearwater and cormorant from the Horcon Formation. Proximal fragment of a fossil left tarsometatarsus assigned as *Puffinus* cf. *griseus* (SGO-PV 21490) in (**A**) dorsal, (**C**) plantar and (**E**) proximal views; and (**F**) sketch showing the details of the proximal surface. Proximal section of the same element in the extant great shearwater (*Puffinus gravis*) in (**B**) dorsal, (**D**) plantar and (**G**) proximal views. Partial wings and pectoral girdle of the small cormorant *Phalacrocorax* sp. (SGO-PV 21443): (**H**) fragment of right ulna in dorsal view; (**I**) right coracoid in dorsal view; (**J**) proximal fragment of left scapula in medial; (**K**) left coracoid in ventral view; (**L**) proximal fragment of left humerus in caudal view; (**M**) left radius lacking of proximal end in ventral view; (**N**) left ulna lacking of proximal end in ventral view; and (**O**) proximal fragment of left carpometacarpus in ventral view.
doi:10.1371/journal.pone.0090043.g004

complete specimens in the Pisco Formation. This unnamed taxon was the most common cormorant along the coast of Chile and Peru during the late Neogene.

Discussion

The South American Record of seabirds during the Pliocene

The fossil record of seabirds during the Pliocene in the Southeastern Pacific has been mostly restricted to the area currently comprised by the PCP, and the Horcon assemblage is the first fauna described for the transitional zone and the southernmost seabird locality currently known for the Pliocene of South America (Figure 5B).

After the recent publication of new radiometric dates for the vertebrate horizons Sacaco and Sacaco Sur from the Pisco Formation [50], the only possibly Pliocene locality from Southern Peru is Yauca [51,52]. If this age can be confirmed, this locality will be the most diverse seabird assemblage for this interval in South America, including penguins, cormorants and petrels, along with at least three species of boobies currently unrecorded in other areas [7,51,53]. A minimum of three other localities is known in Northern Chile. These are the outcrops of the La Portada Formation in Mejillones [16], the Pliocene Lechero Member of the Bahia Inglesa Formation at Los Negros locality [37,54], and the Carrizal locality of the Coquimbo Formation [18]. It is possible that the record from Coquimbo [17] also belongs to the Pliocene levels of the Coquimbo Formation. Penguins are abundant and diverse across these localities, whereas the record of other families is comparatively rare and includes petrels, albatrosses, cormorants and caracaras.

Although the Pliocene record consists exclusively of extant families, the seabird assemblages from Chile and Peru are composed of a mixture of modern and extinct taxa. In comparison with the Late Miocene, the only suprageneric taxon currently absent from the Pliocene record is the Pelagornithidae, whereas the great booby *Sula magna* persists in Southern Peru [51], and the small cormorant *Phalacrocorax* sp. is still present from Peru to the transitional zone [7,16]. It is possible that only one of the up to five Late Miocene species of penguins persisted until the Pliocene: the medium-sized *Spheniscus* sp. recorded in Yauca and Carrizal [18,53]. On the other hand, at least three extant species are possibly present during the Pliocene: the Humboldt penguin *Spheniscus humboldti* [53], the Guanay cormorant *Phalacrocorax bougainvillii* [7], and the sooty shearwater *Puffinus* cf. *griseus* recorded in Horcon. The first two species are endemic to the PCP, whereas the last one has a wide dispersion range but only breeds in Subantarctic regions including the Magellanic region in South America [10]. This suggests that the processes that originated the modern seabird faunas along the Pacific coast of South America had already started in the Late Pliocene; however, most of them remain minor elements in the Pliocene assemblages.

Comparing the current and Pliocene richness of penguins and cormorants across the PCP and the transition zone (Figure 5A), we can see a general increase in the case of the cormorants, and a decrease in the diversity of penguins in Peru and Northern Chile. Similarly to the situation described for the North Pacific prior the Pliocene [55], cormorants are comparatively rare in the record of Peru and particularly Chile. Two species are known from the Late Miocene to the Pliocene, whereas no fewer than three are currently present across the Humboldt System. The small Neogene cormorant *Phalacrocorax* sp., a possible ecological analogue of the Red-legged Cormorant *P. gaimardi*, is by far the most common cormorant until the Late Pliocene, whereas

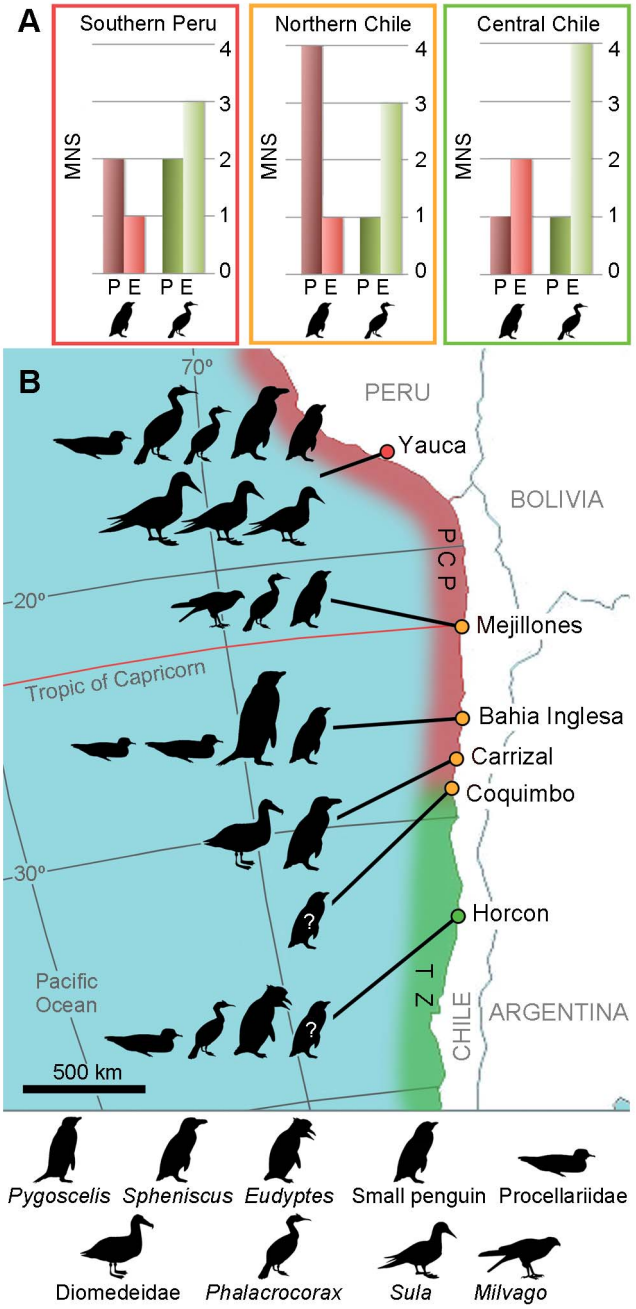

Figure 5. The Pliocene record of birds in the Southeast Pacific. **A.** Comparison between the Pliocene (P) and extant (E) richness of penguins and cormorants for each major area represented as minimum number of species (MNS); **B.** Map showing the main fossiliferous localities, the zoogeographical regions (PCP, Peruvian–Chilean Province; TZ, Transition Zone) and the species recorded.
doi:10.1371/journal.pone.0090043.g005

specimens identifiable as the Guanay cormorant *P. bougainvillii* are scarce. In contrast, the Guanay cormorant is currently one of the most abundant and main guano-producing species in the PCP [56], and it is also the most abundant species in Pleistocene sites of southern Peru [57]. This change in dominance is most likely related to the warmer oceanic conditions during the Pliocene [58], and their effect on the main prey of the Guanay: the Peruvian anchovy. Warm periods, like El Niño events, have a negative effect on the population of anchovy and drive the alternate regimen

shifts between this species and the sardine [59]. Drops in the anchovy population have strong effects on the population of the Guanay cormorant and, in combination with commercial fishing, had been associated with the recent decline of that species [60]. The predominance of warmer waters in the Pliocene of Northern and Central Chile (see [61]) represents an adverse scenario for these species.

On the other hand, only two species of penguins remained in Peru by the Pliocene and a minimum of four were present across Northern Chile, whereas the Humboldt penguin is the only species that currently inhabits this area. This decrease in the diversity of penguins is not well recorded in Horcon, where two species of banded penguins can currently be found and only one species of crested penguin can be confirmed for the Pliocene. Small penguins in the size range of the Humboldt penguin became more common in Northern Chile, and remains of medium sized *Spheniscus* are comparatively rare during the Pliocene, whereas slightly larger species like *S. urbinai* were common across the PCP during the Late Miocene. However, at least one species, "*Pygoscelis*" *grandis*, reached a large size in the range of *Aptenodytes*. This relatively high diversity of penguins is intriguing considering the warmer conditions described for the Pliocene [58,61,62]. Nevertheless, there is also a reduction in size and a drop in the richness of species with respect to the Late Miocene, where a minimum of four species can be found in the Bahia Inglesa bonebed [3,18]. Interestingly, no more than two species have been found at the same locality in the Pliocene in Northern Chile.

Subantarctic seabirds during the Pliocene Warming

The possible presence of genera currently restricted to the Subantarctic and Antarctic in lower latitudes is another enigmatic characteristic of seabird faunas during the Pliocene. Despite the existence of other Neogene species originally attributed to the Antarctic genera *Pygoscelis* [37,63,64] and *Aptenodytes* [63], *Eudyptes calauina* is the only one currently supported by phylogenetic analysis as part of a Subantarctic genus (see [41]). The presence of subadults and possibly juveniles indicates that this was a breeding species in Central Chile. Currently, the Southern Rockhopper and Macaroni penguins are the only two breeding species in South America, with colonies restricted to austral islands over 50°S [65]. Nevertheless, most of the crested penguins breed on islands surrounding New Zealand between 35 and 55°S [66], in waters with average Sea Surface Temperatures (SST) between 15 and 7°C. Multiproxy reconstructions and climate modeling suggest SST around 16°C during the austral winter and 20°C during summer in central Chile during the Pliocene [67]. However, there is currently no Pliocene data available that comes directly from the Humboldt Current System. The living crested penguins are migratory and highly seasonal breeders [66]. This suggests that *E. calauina* was a migratory species, probably breeding during the austral winter like the Northern Rockhopper and the Fiordland penguin [68]; and adapted to warmer conditions than the species that currently inhabit South America, being probably more similar to the New Zealand species. This may also be one of the causes for the disappearance of this species from the transitional zone with the beginning of Quaternary cooling.

The Benguela Current system in South Africa is the only other area with a well-known Pliocene record of seabirds in the South Hemisphere [1,30,69]. Seals [70] and a high diversity of penguins [30] and Procellariiformes, including prions (*Pachyptila*) and diving petrels (*Pelecanoides*) [71], are known for this region and have been interpreted as evidence of Subantarctic conditions [1,69]. This seems to contradict the warmer temperatures currently known for the Pliocene [58,61,62,67]. However, it is possible that the meaning of this vertebrate assemblage in terms of cooler temperatures has been overstated, being also congruent with temperate conditions. Seals are a dominant element of the pinniped assemblages during the Neogene in the Southern Hemisphere [54], being diverse under the warmer climate of the Miocene. Despite the fact that prions mainly breed in Subantarctic islands, many species, like the Fairy and Broad-billed prions [72], also breed in temperate areas. Furthermore, the Magellanic Diving-petrel is the only diving petrel truly restricted to cold-temperate regions, whereas two of the remaining species reach warm-tempered areas and one, the Peruvian Diving-petrel, is completely restricted to the PCP [72]. Finally, multiproxy reconstructions suggest SST around 18°C during winter and 22°C during summer in the Western Cape of South Africa for the Late Pliocene [67], being a similar range to the current summer conditions at the area.

There is no doubt that, as in South America, the fossil assemblages of South Africa show significant differences with respect to the faunas that currently inhabit the region. Furthermore, the South African seabird assemblage during the Pliocene was apparently more similar to the extant assemblage of the South American PCP. Boobies (*Sula*), the dominant sulid genus during the Neogene and the only one still present in South America, were also present during the Pliocene in South Africa and later replaced by the Cape gannet *Morus capensis* [1,69]. Diving petrels and several species of storm petrels have been identified as endemic species present in the Humboldt system without an ecological equivalent in the present-day Benguela system [73]; whereas at least one species of diving petrel and two of storm petrels were present during the Pliocene [71]. The disappearance of these cold/temperate elements from South Africa is intriguing considering the cooling trend of this region. Current estimations suggest that the drop in SST was stronger and faster in the Benguela than in the Humboldt system: approximately 8°C in 3.3 Ma versus 4°C in 3.8 Ma [62]. One of the main drivers proposed for this faunal turnover is the change in the availability of breeding areas (islands and/or beaches) due to sea level fluctuation [1,30,54,71]. This is certainly a possible explanation for a global reduction in the richness of Procellariiformes and penguins, which largely prefer islands to continental beaches. On the other hand, the differential extinction of cold/temperate birds in the Benguela and Humboldt systems can be related to the larger latitudinal thermal gradient in South America, which allows these taxa to expand or contract their distribution more easily than in Southern Africa. In this sense, the mixed seabird fauna of Horcon shows that at least some seabirds species, like the small Neogene cormorant, where spread across a wide range of climatic conditions during the Pliocene. Additionally, it is possible that the difference in the SST cooling rate [62] could also play a role in this differential extinction.

Conclusion

The fossil record of Horcon reflects the existence of a mixed seabird fauna in central Chile during the Pliocene, resembling the current assemblages from the transitional zone. This area is unique through the presence of *E. calauina*, the oldest record of this genus, which is currently absent from the Humboldt System but present in the Magellanic region. It also includes the first Pliocene record of the sooty shearwater that currently breeds in the Magellanic region, and a small cormorant shared with Southern Peru and Northern Chile. The presence of a transitional zone in central Chile during the Pliocene is congruent with the comparatively cooler conditions suggested for Southern Chile based on foraminifera [74], and the annual temperature oscillation that could affect the area according to multiproxy reconstructions [67]. This thermal gradient could also play an important role in the

preservation of a higher diversity of cold/temperate seabirds in the Humboldt Current, compared with similar upwelling systems like the Benguela Current (west coast of southern Africa). Nevertheless, it is clear that despite the latitudinal differences across the Humboldt System, the Pliocene seabirds represent a distinctive assemblage linking the living faunas with the Late Miocene forms. At the moment, the lack of Neogene records in Southern Chile prevents us from making more detailed comparisons with the Magellanic region, but it is expected that this gap can be filled in the near future.

Supporting Information

Document S1 Complementary information, Figures S1–S3 and Table S1. Stratigraphic column. Expanded anatomical description. Phylogenetic analysis including details about the changes introduced to the original data set, GenBank accession numbers and authorships, list of morphological characters, and list of osteological synapomorphies. Figure S1: Location map and stratigraphic column of the Horcon Formation. Figure S2: Detail of bone surface texture in penguin specimens. Figure S3: Complementary strict and Adams consensus trees from combined and morphology-only analyses. Table S1: Comparative measurements for the tarsometatarsus.
(PDF)

Dataset S1 Phylogenetic analysis matrix.
(NEX)

Acknowledgments

We thank Rodolfo Salas from the Museo de Historia Natural de la Universidad Nacional de San Marcos (Lima, Peru), Eberhard Frey from the Staatliches Museum für Naturkunde Karlsruhe (Karlsruhe, Germany) and Sylke Frahnert and Pascal Eckhoff from the Museum für Naturkunde (Berlin, Germany) for facilitating the access to important comparative specimens. To Rafael Varas, Ali Altamirano and Jose Grau for their help during the visit of MCH to the collections in Peru and Germany. Thanks are also given to David Rubilar Rogers from the Museo Nacional de Historia Natural (Santiago, Chile) who facilitated the deposit of the specimens. To María Verónica Andrade and the Museo de Historia Natural de Puchuncaví (Puchuncaví, Chile) for their collaboration during the fieldwork. Antoine Louchart and Daniel Ksepka help to improve this paper. Finally we want to thank Michael Benton for his support.

Author Contributions

Conceived and designed the experiments: MCH JCB SNN. Performed the experiments: MCH. Analyzed the data: MCH. Wrote the paper: MCH JCB SNN. Field work: JCB SNN. Preparation of specimens: JCB. Geological study and construction of stratigraphic column: JCB SNN. Provided the original illustrations: MCH.

References

1. Warheit K (2002) The seabird fossil record and the role of paleontology in understanding seabird community structure. In: Schreiber E, Burger J, editors. Biology of marine birds. Florida: CRC Press. pp. 17–55.
2. Walsh S, Hume J (2001) A new Neogene marine avian assemblage from north-central Chile. Journal of Vertebrate Paleontology 21: 484–491.
3. Chávez Hoffmeister M (2007) Observaciones sobre la presencia de *Paraptenodytes* y *Palaeospheniscus* (Aves: Sphenisciformes) en la Formación Bahía Inglesa, Chile. Revista Chilena de Historia Natural 80: 255–259.
4. Mayr G, Rubilar-Rogers D (2010) Osteology of a new giant bony-toothed bird from the Miocene of Chile, with a revision of the taxonomy of Neogene Pelagornithidae. Journal of Vertebrate Paleontology 30: 1313–1330.
5. Cheneval J (1993) L'avifaune Mio-Pliocène de la Formation Pisco (Pérou) étude préliminaire. Documents des Laboratoires de Géologie de Lyon 125: 85–95.
6. Stucchi M (2002) Una nueva especie de *Spheniscus* de la Formación Pisco, Perú. Boletín de la Sociedad Geológica del Perú 94: 19–6.
7. Urbina M, Stucchi M (2005) Los Cormoranes (Aves: Phalacrocoracidae) de la Formación Pisco, Perú. Boletín de la Sociedad Geológica del Perú 99: 41–49.
8. Thiel M, Macaya EC, Acuña E, Arntz WE, Bastias H, et al. (2007) The Humboldt Current System of Northern and Central Chile: oceanographic processes, ecological interactions and socioeconomic feedback. Oceanography and Marine Biology Annual Review 45: 195–344.
9. Briggs J (1974) Marine Zoogeography. New York: McGraw-Hill Book Company. 475 p.
10. Schlatter RP, Simeone A (1999) Estado del conocimiento y conservación de las aves en mares chilenos. Estudios Oceanológicos 18: 25–33.
11. Hartmann-Schröder VG, Hartmann G (1962) Zur Kenntnis de Eulitorals der chilenischen Pazifikküste und der argentinischen Küste Südpatagoniens unter besonderer Berücksichtigung der Polychaeten und Ostracoden. Mitteilungen aus dem Hamburgischen Zoologischen Museum und Institut. Ergänzungsband zu Band 60: 270.
12. Knox GA (1960) Littoral ecology and biogeography of the Southern Ocean. In: Pantin CFA, editors. A discussion of the biology of the southern cold temperate zone London: Proceedings of the Royal Society B 152: 577–624.
13. Camus PA (2001) Biogeografía marina de Chile continental. Revista Chilena de Historia Natural 74: 587–617.
14. Stucchi M, DeVries T (2003) El registro más antiguo de Sulidae en el Perú. Boletín de la Sociedad Geológica del Perú 96: 117–120.
15. Acosta Hospitaleche C, Stucchi M (2005) Nuevos restos terciarios de Spheniscidae (Aves, Sphenisciformes) procedentes de la costa del Perú. Revista Española de Paleontología 20: 1–5.
16. Emslie S, Guerra Correa C (2003) A new species of penguin (Spheniscidae: *Spheniscus*) and other birds from the late Pliocene of Chile. Proceedings of the Biological Society of Washington 116: 308–316.
17. Acosta Hospitaleche C, Canto J, Tambussi C (2006) Pingüinos (Aves, Spheniscidae) en Coquimbo (Mioceno medio- Plioceno superior), Chile y su vinculación con las corrientes oceánicas. Revista Española de Paleontología 21: 115–121.
18. Chávez Hoffmeister M (2007) Fossil birds of Chile and Antarctic Peninsula. Archivos do Museu Nacional Rio de Janeiro 65: 551–572.
19. Thomas H (1958) Geología de la Cordillera de la costa entre el Valle de La Ligua y La Cuesta de Barriga. Boletín del Instituto de Investigaciones Geológicas 2: 1–86.
20. Tavera J (1960) El Plioceno de Bahía Horcón en la provincia de Valparaíso. Facultad de Ciencias Físicas y Matemáticas, Universidad de Chile, Anales 17: 346–367.
21. Carrillo-Briceño JD, González-Barba G, Landaeta MF, Nielsen SN (2013) Condrictios fósiles del Plioceno Superior de la Formación Horcón, Region de Valparaíso, Chile central. Revista Chilena de Historia Natural 86: 191–206.
22. Herm D (1969) Marines Pliozän und Pleistozän in Nord- und Mittel-Chile unter besonderer Berücksichtigung der Entwicklung der Mollusken-Faunen. Zitteliana 2: 1–159.
23. DeVries TJ (1997) A review of the genus *Chorus* Gray, 1847 (Gastropoda: Muricidae) from Western South America. Tulane Studies in Geology and Paleontology 30: 125–145.
24. DeVries TJ (2005) Late Cenozoic Muricidae from Peru: Seven New Species and a Biogeographic Summary. The Veliger 47: 277–293.
25. DeVries TJ, Vermeij GJ (1997) *Herminespina*: new genus of Neogene muricid gastropod from Peru and Chile. Journal of Paleontology 71: 610–615.
26. Frassinetti D (2000) Moluscos del Plioceno Superior marino de Isla Guafo, sur de Chile. Parte II. Gastropoda. Boletín del Museo Nacional de Historia Natural 49: 131–161.
27. Griffin M, Nielsen SN (2008) A revision of the type specimens of Tertiary molluscs from Chile and Argentina described by d'Orbigny (1842), Sowerby (1846) and Hupé (1854). Journal of Systematic Palaeontology 6: 251–316.
28. Nielsen SN (2013) A new Pliocene mollusk fauna from Mejillones, northern Chile. Paläontologische Zeitschrift 87: 33–66.
29. Ksepka DT, Fordyce RE, Ando T, Jones CM (2012) New fossil penguins (Aves: Sphenisciformes) from the Oligocene of New Zealand reveal the skeletal plan of stem penguins. Journal of Vertebrate Paleontology 32: 235–254.
30. Ksepka DT, Thomas DB (2012) Multiple Cenozoic invasions of Africa by penguins (Aves, Sphenisciformes). Proceedings of the Royal Society B 279: 1027–1032.
31. Swofford DL (2003) PAUP. Phylogenetic Analysis Using Parsimony (and Other Methods). SinauerAssociates, Sunderland, Massachusetts.
32. Warheit K (1992) The Role of Morphometrics and Cladistics in the Taxonomy of Fossils: A Paleornithological Example. Systematic Biology 41: 345–369.
33. Worthy TH (1997) The identification of fossil *Eudyptes* and *Megadyptes* bones at Marfells Beach, Marlborough, South Island. New Zealand Natural Sciences 23: 71–85.
34. Tumarkin-Deratzian AR, Vann DR, Dodson P (2006) Bone surface texture as an ontogenetic indicator in long bones of the Canada goose *Branta canadensis*. Zoological Journal of the Linnean Society 148: 133–168.
35. Göhlich U (2007) The oldest fossil record of the extant penguin genus *Spheniscus*, a new species from the Miocene of Peru. Acta Palaeontologica Polonica 52: 285–298.

36. Acosta Hospitaleche C, Tambussi C, Donato M, Cozzuol M (2007) A new Miocene penguin from Patagonia and its phylogenetic relationships. Acta Palaeontologica Polonica 52: 299–314
37. Walsh SA, Suárez ME (2006) New penguin remains from the Pliocene of northern Chile. Historical Biology 18: 115–126.
38. Ksepka DT, Bertelli S, Giannini N (2006) The phylogeny of the living and fossil Sphenisciformes (penguins). Cladistics 22: 412–441.
39. Subramanian S, Beans-Picón G, Swaminathan S, Millar C, Lambert D (2013) Evidence for a recent origin of penguins. Biology Letters 9: 20130748.
40. Baker AJ, Pereira SL, Haddrath OP, Edge A (2006) Multiple gene evidence for expansion of extant penguins out of Antarctica due to global cooling. Proceedings of the Royal Society B 217: 11–17
41. Ksepka DT, Clarke JA (2010) The basal penguin (Aves: Sphenisciformes) *Perudyptes devriesi* and a phylogenetic evaluation of the penguin fossil record. Bulletin of the American Museum of Natural History 337: 1–77.
42. Ksepka DT, Ando T (2011) Penguins past, present, and future: trends in the evolution of the Sphenisciformes. In: Dyke G, Kaiser G, editors. Living Dinosaurs, The Evolutionary History of Modern Birds pp. 155–186.
43. Livezey BC (1989) Morphometric patterns in Recent and fossil penguins (Aves, Sphenisciformes). Journal of Zoology 219: 269–307.
44. Stucchi M, Urbina M (2005) Nuevos restos de Procellariiformes (Aves) de la Formación Pisco, Perú. Boletín de la Sociedad geológica del Perú 100: 67–77.
45. Sallaberry M, Rubilar D, Suárez M (2006) El cráneo de un nuevo procelárido (Aves: Procellariidae) del Neógeno (Mioceno Tardío) del desierto de Atacama. Biological Research 39: 4 supl. B, R-94.
46. Howard H (1971) Pliocene avian remains from Baja California. Contributions in Science Los Angeles County Museum 217: 1–17.
47. Howard H (1949) New avian records for the Pliocene of California. Carnegie Instuitution of California 584: 179–200.
48. Chandler RM (1990) Fossil birds of the San Diego Formation, Late Pliocene, Blancan, San Diego County, California. Ornithological Monographs 44: 73–161.
49. Chávez Hoffmeister M, Stucchi M, Urbina M (2007) El registro de Pelagornithidae (Aves: Pelecaniformes) en el Pacifico Sudeste. Bulletin de l'Institut Français d'Etudes Andines 36: 175–197.
50. Ehret DJ, MacFadden BJ, Jones DS, Foster DA, Salas-Gismondi R (2012) Origin of the white shark *Carcharodon* (Lamniformes: Lamnidae) based on recalibration of the Upper Neogene Pisco Formation of Peru. Paleontology 55: 1139–1153.
51. Stucchi M (2003) Los Piqueros (Aves: Sulidae) de la Formación Pisco, Perú. Boletín de la Sociedad Geológica del Perú 95: 75–91.
52. Muizon C, de, McDonald HG, Salas R, Urbina M (2004) The evolution of feeding adaptations of the aquatic sloth *Thalassocnus*. Journal of Vertebrate Paleontology 24: 398–410.
53. Stucchi M (2007) Los pingüinos de la Formación Pisco (Neógeno), Perú. In: Díaz-Martínez E, Rábano I, editors. IV European Meeting on the Paleontology and Stratigraphy of Latin America. Madrid: Instituto Geológico y Minero de España.
54. Valenzuela Toro AM, Gutstein CS, Varas Malca RM, Suarez ME, Pyenson ND (2013) Pinniped turnover in the South Pacific Ocean: new evidence from the Plio-Pleistocene of the Atacama Desert, Chile. Journal of Vertebrate Paleontology 33: 216–223.
55. Warheit KI (1992) A review of the fossil seabirds from the Tertiary of the North Pacific: plate tectonics, paleoceanography, and faunal change. Paleobiology 18: 401–424.
56. Weimerskirch H, Bertrand S, Silva J, Bost C, Peraltilla S (2012) Foraging in Guanay cormorant and Peruvian booby, the major guano-producing seabirds in the Humboldt Current System. Marine Ecology Progress series 458: 231–245.
57. DeFrance SD (2005) Late Pleistocene marine birds from southern Peru: distinguishing human capture from El Niño-induced windfall. Journal of Archaeological Science 32: 1131–1146.
58. Dowsett HJ, Robinson MM, Haywood AM, Hill DJ, Dolan AM, et al. (2012) Assessing confidence in Pliocene sea surface temperatures to evaluate predictive models. Nature Climate Change 2: 365–371.
59. Alheit J, Niquen M (2004) Regime shifts in the Humboldt Current ecosystem. Progress in Oceanography 60: 201–222.
60. Duffy D (1983) Environmental uncertainty and commercial fishing: effects on Peruvian Guano birds. Biological Conservation 26: 227–238.
61. Le Roux JP (2012) A review of Tertiary climate changes in southern South America and the Antarctic Peninsula. Part 1: Oceanic conditions. Sedimentary Geology 247: 1–20.
62. Fedorov AV, Brierley CM, Lawrence KT, Liu Z, Dekens PS, et al. (2013) Patterns and mechanisms of early Pliocene warmth. Nature 496: 43–49.
63. Simpson G (1972) Pliocene penguins from North Canterbury, New Zealand. Records Canterbury Museum 9: 159–182.
64. Acosta Hospitaleche C, Chávez Hoffmeister M, Fritis O (2006) Pingüinos fósiles (*Pygoscelis calderensis* nov. sp.) en la Formación Bahía Inglesa (Mioceno Medio - Plioceno), Chile. Revista Geológica de Chile 33: 327–338.
65. Oehler DA, Pelikan S, Fry WR, Weakley L Jr, Kusch A, et al. (2008) Status of Crested Penguin (*Eudyptes* spp.) populations on three islands in Southern Chile. The Wilson Journal of Ornithology 120: 575–581.
66. Davis LS, Renner M (2003) Penguins. New Haven: Yale University Press. 212 p.
67. Dowsett HJ, Robinson MM, Foley KM (2009) Pliocene three-dimensional global ocean temperature reconstruction. Climate of the Past 5: 769–783.
68. Garcia P, Boersma PD (2013) Penguins, natural history and conservation. Seattle: University of Washington Press. 328 p.
69. Olson SL (1983) Fossil seabirds and changing marine environments in the Late Tertiary of South Africa. South Africa Journal of Science 73: 399–402.
70. Avery G, Klein RG (2011) Review of fossil phocid and otariid seals from the southern and western coasts of South Africa. Transactions of the Royal Society of South Africa 66: 14–24.
71. Olson SL (1985) Early Pliocene Procellariiformes (Aves) from Langebaanweg, South-Western Cape Province, South Africa. Annals of the South African Museum 95: 123–145.
72. Harrison P (1985) Seabirds, an identification guide. London: Christopher Helm. 448 p.
73. Crawford RJM, Goya E, Roux JP, Zavalaga CB (2006) Comparison of assemblages and some life-history traits of seabirds in the Humboldt and Benguela systems. African Journal of Marine Science 28: 553–560.
74. Forsythe RD, Olsson R, Johnson C, Nelson E (1985) Stratigraphic and micropaleontologic observations from the Golfo de Penas-Taitao Basin, Southern Chile. Revista Geológica de Chile 25: 3–12.

Document S1 - Chávez Hoffmeister et al. The evolution of seabirds in the Humboldt Current: New clues from the Pliocene of central Chile

Stratigraphic column

Two well-defined stratigraphic intervals can be identified across the entire sequence. The lower unit crops out with an estimated thickness of less than 8 m and consists of a sequence of conglomerates and greenish glauconitic sandstones containing some white calcareous concretions. The presence of carbonized plant remains and the absence of macrofossils are also characteristic of this unit. The upper unit corresponds to the main section of the sequence. The lithology of this unit is characterized by layers of fine to coarse sandstone, light-colored and poorly consolidated, which are interspersed with few conglomeritic layers.

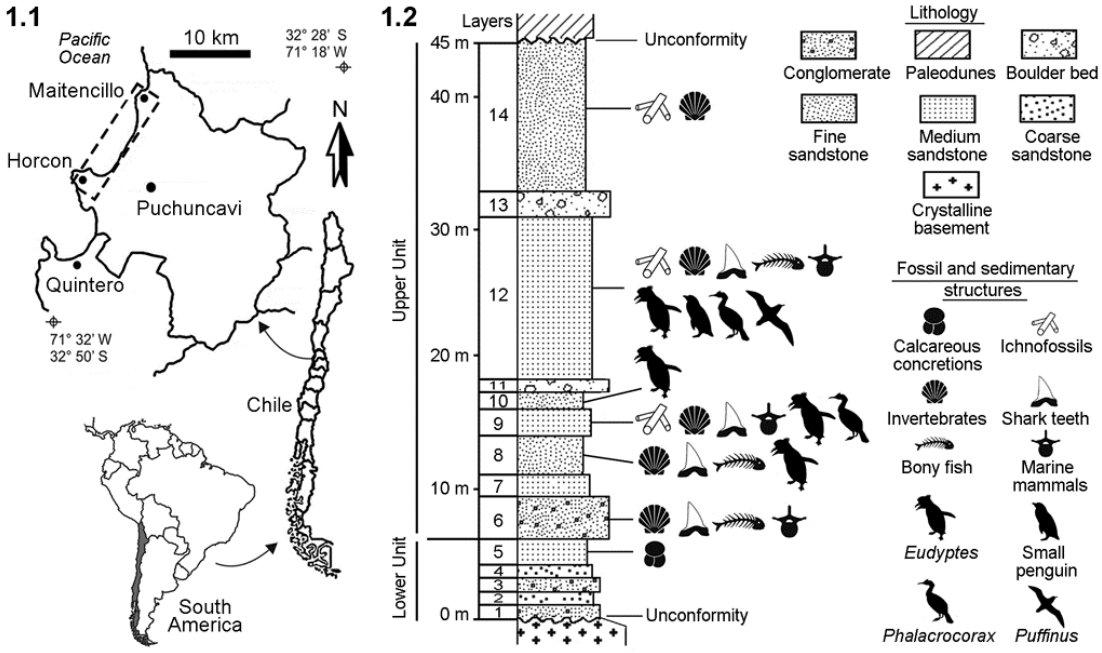

Figure S1.1. Location map. **S1.2.** Stratigraphic column of the Horcon Formation.

Expanded anatomical description

Vertebrae

SGO-PV 21452 is most likely a fourth cervical. Its general shape resembles those observed in *Eudyptes chrysocome*, *E. chrysolophus* and *Madrynornis*. The dorsal tori are strongly prominent, relatively narrow anteroposteriorly and with their extremities pointing laterocaudally as in the compared species of *Eudyptes* and *Madrynornis*; whereas in *Spheniscus urbinai* the tori of module 3 and 4 (sensu Guinard et al. 2010) are less prominent, more rounded and wider anteroposteriorly. The hypapophysis is larger than in compared species of the genus, relatively slender and ventrocaudally directed.

Humerus

Based on SGO-PV 21449 and the section preserved in SGO-PV 21451, the head is strongly prominent proximally and has the shape of a rampant arch with the apex ventrally located in posterior view; whereas in *Eudyptula* and *Spheniscus* the head is less prominent, giving a flatter appearance to the proximal extreme of the humerus. In SGO-PV 21451, a notch between the dorsal tubercle and the base of the humeral head is clearly visible in caudal view (Figure 1d). This notch is usually absent in *Spheniscus*, *Eudyptula* and *Tereingaornis.* In SGO-PV 21449, the capital incisure is completely separated from the transverse ligament sulcus as in *Eudyptes*, *Spheniscus* and *Eudyptula* (Figure 1e). However, these are connected by a sulcus in *Aptenodytes*, *Inguza*, *Madrynornis*, *Palaeospheniscus* and *Eretiscus.* A deep pit for ligament insertion is present on the proximal surface adjacent to the head as in most Spheniscidae. This pit is

absent or extremely shallow in *Pygoscelis*, *Madrynornis*, *Palaeospheniscus*, *Eretiscus* and occasionally in *Aptenodytes patagonicus.* The proximal margin of the tricipital fossa is weakly projected in proximal view as in most living and Neogene penguins, like *Madrynornis*, *Inguza* and *Palaeospheniscus*. In contrast, it develops a lip-like projection that is well exposed in proximal view in extant species of *Spheniscus* and occasionally in *Pygoscelis antarctica*. Unlike the living species of *Eudyptes* and *Spheniscus chilensis*, where the proximal border of the tricipital fossa forms a symmetrical concavity in ventral view; in *E. calauina* it is asymmetrical and slightly concave. The impressio insertii m. supracoracoideus and m. latissimus dorsi are separated by a small gap as in Spheniscidae. The shaft robustness index (SRI: proximodistal length / ventrodorsal width at middle point, see Character 176) shows a value (4) at the limit between most of the living penguins (4.1-4.9) and the bulkiest fossil taxa such as *Paraptenodytes robustus* (MACN A-11032, holotype of *Isotremornis nordenskjoldi*) (3.9), *Pachydyptes* (3.8) and *Platydyptes novaezealandiae* (3.6). The nutrient foramen is situated on the ventral face of the shaft as in *Palaeospheniscus* and all Spheniscidae, whereas in *Madrynornis* and *Eretiscus* it is situated on the anterior face. The dorsal edge of the shaft is curved and without a clear preaxial angle as is usual in *Eudyptes*, nevertheless, a well-defined angle can occasionally be found as the normal condition in *Aptenodytes*, *Pygoscelis*, *Megadyptes*, *Spheniscus*, *Palaeospheniscus* and *Eretiscus*. The posterior trochlear ridge reaches the ventral edge of the shaft. This condition is also present in living species of *Eudyptes*, *Megadyptes* and *Palaeospheniscus*; where as a result, the ridge often slightly exceeds the ventral margin in cranial view but not in caudal view. In *Aptenodytes, Pygoscelis* and *Madrynornis* the ridge extends beyond the ventral margin, but does not

reach the ventral edge in *Inguza, Eretiscus* and most species of *Spheniscus*. The trochlear angle measured in SGO-PV 21451, defined as the angle between the main axis of the shaft and the tangent of ventral and dorsal condyles, is equal to 45°. This angle is within the range of most Spheniscidae (greater than or equal to 45°), although it is smaller in *Inguza* (43°), *Madrynornis* (41°) and *Tereingaornis* (41°); and occasionally in *Spheniscus urbinai* (43°-52°)*, Palaeospheniscus* (39°-49°) and *Eretiscus* (44°-54°). In ventral view, the ventral condyle is almost parallel to the dorsal condyle and does not extend the anterior edge of the humerus which is flattened as in most Spheniscidae. In *Madrynornis*, *Palaeospheniscus* and *Eretiscus* the ventral condyle is more rounded and slightly surpasses the anterior edge. The dorsal end of the scapulotricipital sulcus is curved caudally and completely separated from the humerotricipital sulcus by the medial trochlear ridge; as in *Aptenodytes*, *Spheniscus muizoni*, *Madrynornis*, *Palaeospheniscus* and *Eretiscus*. In other species of *Eudyptes* and *Spheniscus,* the dorsal end of the scapulotricipital sulcus is dorsally connected to the humerotricipital sulcus.

Tibiotarsus

The proximal fragment of a tibiotarsus SGO-PV 21447 (Figure 1h) partially resembles that of *S. megaramphus*. However, it is much smaller than in that species and many of their similarities are shared with other Spheniscidae, including *Eudyptes*. Similar to *Spheniscus* or *Aptenodytes*, the lateral crest is strongly prominent cranially in lateral view, unlike *Eudyptes* where the cranial edge of the crest is almost aligned with the cranial edge of the diaphysis. The cranial margin of the lateral crest is thickened but delimited by the proximal and distal edges of the crest shaft, whereas in *Spheniscus,*

Eudyptes, *Madrynornis* and *Palaeospheniscus* the margin is often projected proximally creating a proximal prominence in lateral view. The lateral longitudinal flexor fossa is relatively well developed and clearly delimited medially by a longitudinal crest, whereas the medial fossa of the collateral ligament is shallow and medially open as in most of the extant penguins. In *S. muizoni* and *Spheniscus* sp. MUSM 800 the collateral ligament fossa is deep and medially enclosed by a short proximal ridge. In the distal fragment of tibiotarsus SGO-PV 21488 (Figure 1i) the sulcus extensorius is located close to the midline of the shaft. The distal epiphysis is relatively wide mediolaterally to a similar degree as in living species of *Eudyptes* and less than in *Megadyptes*. The tubercle for the retinaculum of the fibularis muscle is well defined and prominent in caudal view. As in *Eudyptes*, *S. chilensis*, *Madrynornis* and *Palaeospheniscus*; a tuberosity for the extensor reticulum appears in the lateral edge forming a shallow lip-like crest. This tuberosity is usually absent in *Spheniscus* and occasionally present in *Aptenodytes* and *Pygoscelis* (Göhlich, 2007). The caudal edge of the medial condyle is slightly damaged. However, the edge is apparently continuous also in medial view, unlike in *S. chilensis* and *Eudyptes* where it is distally notched (Göhlich, 2007). In cranial view, the lateral condyle is slightly inflated laterally as in *Eudyptes* and *Madrynornis* creating a relatively straight lateral edge.

Tarsometatarsus

The surface texture on the holotype SGO-PV 21487 suggest that it can be attributed to an adult, whereas the porous and fibrous textures observed on the tarsometatarsus SGO-PV 21444 allow us to attribute these specimen to a subadult (Figure S2.A-B).

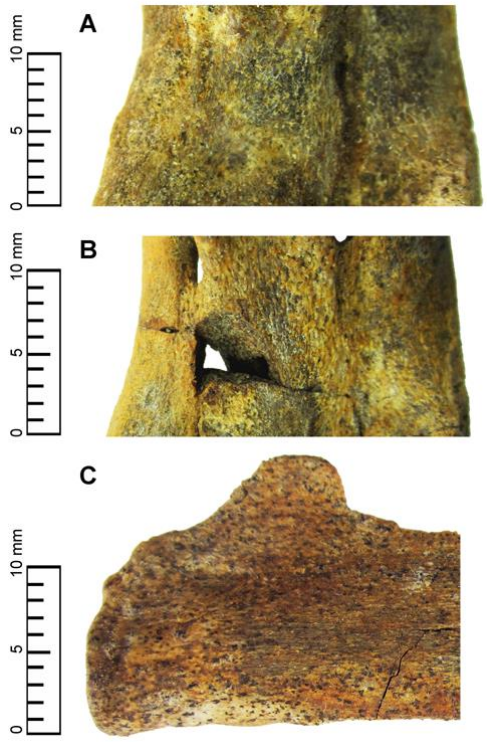

Figure S2. Detail of bone surface texture in penguin specimens. The bones in adults have a smoother surface as can be observed in the holotype of *Eudyptes calauina* SGO-PV 21487 (**A**, plantar). In contrast, the porous and fibrous textures observed on the tarsometatarsus SGO-PV 21444 (**B**, plantar) and the ulna SGO-PV 21455 (**C**, ventral), along with the degree of development of some anatomical features; allow us to attribute these specimens to subadults.

The collateral lateral ligament scar is extremely shallow in SGO-PV 21444 (Figure 1p) and absent in SGO-PV 21487 (Figure 1j) as in *Eudyptes*, *Megadyptes* and *Aptenodytes*. This scar is located proximodorsally in *Spheniscus*, *Eudyptula*, *Inguza*, *Nucleornis*, *Madrynornis*, *Palaeospheniscus* and *Eretiscus;* creating a truncate proximolateral vertex in dorsal view. The intermediate hypotarsal crest is indistinguishable from the lateral crest in plantar view as in all Spheniscidae, while in

Madrynornis, *Palaeospheniscus*, *Eretiscus* and occasionally in *Eudyptula* an extremely shallow groove is visible in proximal view slightly delimited by both crests. As in *Eudyptes*, *Madrynornis*, *Palaeospheniscus*, *Eretiscus* and *Korora*, the lateral hypotarsal crest is well defined in SGO-PV 21487 (Figure 1k) and forms a diagonal ridge that overhangs the lateral foramen, that is slightly less defined in SGO-PV 21444 (Figure 1q). The medial proximal vascular foramen opens plantarly at the medial surface of the medial hypotarsal crest as in *Eudyptes*, *Spheniscus*, *Eudyptula* and *Madrynornis*; whereas in *Pygoscelis* and *Nucleornis* it opens directly at the plantar surface. In SGO-PV 21487 the foramen is relatively large as in *E. chrysolophus* and *Madrynornis*; and is even larger in SGO-PV 21444, being visible in plantar view as in *Megadyptes* and occasionally in *E. chrysocome*. This degree of development is rare in *Spheniscus*, being often smaller as in *Eudyptula*. The lateral proximal vascular foramen is small as in most Spheniscidae, with the exception of *Spheniscus* in which it is occasionally enlarged (this is particularly common in *S. humboldti*). In contrast, the lateral foramen is vestigial in *Eretiscus* and completely absent in *Nucleornis*. The medial dorsal sulcus is moderately deep as in *Eudyptes*, *Megadyptes*, *S. urbinai* and *S. chilensis*. In *E. schlegeli* and *E. sclateri* the sulcus is occasionally shallow as in *Aptenodytes*, *Pygoscelis*, *Madrynornis*, *Palaeospheniscus* and *Eretiscus*. In contrast, in *Eudyptula*, most of the *Spheniscus* species, *Inguza* and *Nucleornis* the sulcus is much deeper. The lateral edge of the metatarsus IV in SGO-PV 21487 is strongly compressed dorsoplantarly creating a sharp edge in lateral view (Figure 1m), as in *Palaeospheniscus*. In plantar view, the lateral intertrochlear notch is proximally deeper than the medial as in *Eudyptes*, the extant *Spheniscus* spp., *S. muizoni*, *Eudyptula*, *Madrynornis* and *Palaeospheniscus*. The

trochlea metatarsi IV is shorter than the trochlea metatarsi II in dorsal view as in *Eudyptes*, *Madrynornis* and *Palaeospheniscus*; whereas in *Aptenodytes*, *Pygoscelis*, *Megadyptes*, *Eudyptula* and *Spheniscus* both are sub-equal. In distal view, the dorsal edges of the trochlea metatarsi III and IV are aligned at the same plane (Figure 1o,u), whereas in extant species of *Spheniscus*, *S. chilensis* and *S. megaramphus*, the trochlea IV is displaced dorsally. Plantarly, the lateral ridge of the trochlea IV is much larger than the medial ridge in distal view, creating a plantar edge that is strongly pointed laterally and flattened medially as in *Eudyptes*, *Pygoscelis*, *S. chilensis*, *S. urbinai*, *S. megaramphus*, *Eudyptula*, *Madrynornis* and *Palaeospheniscus*. Also in distal view, the plantar edge of the trochlea II is slightly deflected plantarly with respect to the plane defined by the most plantar point of the trochleae III and IV (Figure 1o,u), as in *Eudyptes*, *Aptenodytes*, *Pygoscelis*, the extant species of *Spheniscus*, *S. chilensis*, *S. urbinai*, *S. muizoni* and *Madrynornis.* In plantar view, the trochlea II is slightly pointed with parallel medial and lateral edges in SGO-PV 21487 as in *Megadyptes*, *Aptenodytes*, *Eudyptula*, *S. megaramphus*, *Madrynornis* and *Paleospheniscus.* However, in extant species of *Eudyptes* the trochlea II is strongly pointed with a more rounded medial edge or following the medial edge of the tarsometatarsus. An intermediate state can be seen in SGO-PV 21444, where the trochlea II is slightly pointed but the medial edge follows the medial edge of the tarsometatarsus.

Taxon	Specimens	Length	Proximal width	Distal width	Elongation index (EI)
Eudyptes calauina	SGO-PV 21487	41.3	24.3	27.5	1.7
Eudyptes calauina	SGO-PV 21444	41	22.7	25.3	1.8
Eudyptes chrysolophus	(n = 1) [a]	25.1	14.2	17	1.7
Eudyptes moseleyi	Z.2007.065	30.9	15.3	20.5	2
Eudyptes chrysocome	(n = 3) [a]	29	14.8	19.5	1.9
Eudyptes robustus	(n = 18) [b]	29.36	14.73	19.35	1.9
Eudyptes pachyrhynchus	(n = 28) [b]	30.02	15.2	19.75	1.9
Eudyptes sclateri	(n = 19) [b]	31.6	17.03	22	1.8
Eudyptes schlegeli	AMNH 5399	33.3	18.7	22.2	1.8
Megadyptes antipodes	(n = 20) [b]	35.03	18.37	22.94	1.9
Spheniscus humboldti	(n = 2) [a]	35.7	16.6	21.2	1.8
Spheniscus magellanicus	(n = 5) [c]	31.4	15.7	19.72	2
Spheniscus demersus	(n = 8) [a]	32.7	15.6	19.6	2
Spheniscus muizoni	MNHN PPI 147	33.31	16.22	21.53	2
Spheniscus urbinai	MUSM 401	48.76	24.69	30.09	1.9
Spheniscus megaramphus	MUSM 2087	50.97	26.62	34.66	1.9
Eudyptula minor	(n = 3) [a]	22	10.2	13.4	2.1
Pygoscelis adeliae	(n = 18) [c]	32.48	17.09	21.03	1.9
Pygoscelis papua	(n = 9) [c]	32.84	19.31	24.1	1.7
Pygoscelis antarctica	(n = 3) [c]	28.93	16.07	20.3	1.8
Pygoscelis grandis	SGO-PV 1104	49.2	27.33	–	1.8
Aptenodytes patagonicus	(n = 3) [1]	45.5	27.8	33.3	1.6
Aptenodytes forsteri	(n = 3) [1]	45.2	32.3	38.1	1.1
Madrynornis mirandus	MPEF PV 100	36.3	18.1	19.1	2
Inguza predemersus	SAM PQ L23018	27.2	12.8	–	2.1
Nucleornis insolitus	SAM PQ MBD3	40.4	22.4	–	1.8
Palaeospheniscus bergi	(n = 5) [c]	36.4	16.54	20.56	2.2
Palaeospheniscus patagonicus	(n = 3) [c]	40.06	19.07	23.33	2.1
Palaeospheniscus biloculata	(n = 5) [c]	42.1	19.1	24.1	2.2
Eretiscus tonnii	MLP 81-VI-26-1	19.6	8.16	–	2.4

Table S1. Comparative measurements for the tarsometatarsus in millimeters. Sources of measurements: **a.** Stephan (1979), **b.** Worthy (1997), **c.** Acosta Hospitaleche and Gasparini (2007).

Phylogenetic analysis

Modifications to the matrix

During the revision of the original matrix of Ksepka et al. (2012), some inconsistencies between the list of characters and the coded state in the matrix were detected. The state code of characters 91 and 103 as defined in the character list is switched with respect to the states in the matrix; so that the state 0 in the matrix is defined as state 1 in the list and vice versa. Character 98 defines a state 2 that is not used in the matrix. The same happens with the state 0 of character 187. On the other hand, characters 136, 173 and 195 include an extra state in the matrix that is not defined in the character list. Finally, six characters (201, 202, 203, 204, 207 and 208) have different numerations between the list of characters and the matrix. None of these errors had an impact on the original results offered by Ksepka et al. (2012), but they might create serious mistakes when new taxa are added. All these errors have been corrected for the present version and have been also corrected in an update of Ksepka et al. (2012) (see Dryad database).

GenBank molecular sequences

GenBank accession numbers

Taxon	**12S**	**16S**	**COI**	**Cyt-*b***	**RAG-1**
A. forsteri	DQ137187	DQ137147	DQ137185	DQ137225	DQ137246
A. patagonicus	AY139221	DQ137148	DQ137186	AY 138623	DQ 137247
D. capense	X82517	—	—	AF076046	—
D. exulans	DQ137205	DQ137165	DQ137168	DQ137208	DQ137229
E. chrysocome	AY139630	—	DQ525796	—	DQ525776
E. chrysolophus	DQ137197	DQ137157	DQ137171	AF076052	DQ137223
E. filholi	DQ525741	—	DQ525781	—	DQ525761
E. moseleyi	DQ525746	—	DQ525786	—	DQ525766
E. pachyrhynchus	U88007, X82522	DQ 137152	DQ137170	DQ137210	DQ137231
E. robustus	DQ137193	DQ137153	DQ137176	DQ137126	DQ137237
E. schlegeli	DQ137196	DQ137156	DQ137175	DQ137215	DQ137236
E. sclateri	DQ137194	DQ137154	DQ137169	DQ137309	DQ137230
E. minor	NC_004538	DQ137164	DQ137174	NC_004538	DQ137235
G. immer	AF173577	DQ137166	DQ137167	DQ137207	DQ137288
G. stellata	AF173587	AY293618	AY666477	AF158250	—
M. giganteus	X82523	—	—	AF076060	—
M. antipodes	DQ137198	DQ137158	DQ137184	DQ137224	DQ1372245
O. oceanicus	—	—	DQ433048	AF076062	—
O. leucorhoa	—	—	AY666284	AF0706064	—
P. desolata	—	—	—	AF076068	—
P. urinatrix	X82518	—	—	AF076076	DQ881818
P. immutabilis	—	—	DQ433933	PIU48949	—
P. palpebrata	—	—	—	U48943	DQ881822
P. aequinoctialis	—	—	—	U74350	—
P. brevirostris	NC007174	NC007174	NC007174	NC007174	—
P. gravis	AF175572	AF173752	DQ434014	U74354	—
P. adeliae	AF173573	DQ137149	DQ137183	DQ137223	DQ137224
P. antarctica	DQ137190	DQ137150	DQ137181	AF076089	DQ137242
P. papua	DQ137191	DQ137151	DQ137182	AF076090	DQ137243
S. demersus	DQ137199	DQ137159	DQ137177	DQ137217	DQ137238
S. humboldti	DQ137201	DQ137161	DQ137180	DQ137220	DQ137241
S. magellanicus	DQ137200	DQ137160	DQ137178	DQ137218	DQ137239
S. mendiculus	DQ137202	DQ137162	DQ137179	DQ137219	DQ137240
T. melanophrys	AY158677	AY158677	NC_007172	U48955	AY158677

Authorship

12S rDNA: Baker *et al.* (2006): DQ137187, DQ137190–1, DQ137193–4, DQ137196–202, DQ137205; Banks *et al.* (2006): DQ525741, DQ525746, DQ525756; Cooper & Penny (1997): U88007, U88024; García-Moreno *et al*. (unpublished): AY139621, AY139623, AY139630; Stanley & Harrison (1999): X82517–8, X82522–3, X82533; Slack *et al.* (2006): AY158677; NC_004538; Paterson *et al.* (1995): AF173573, AF173577–8. **16S rDNA:** Baker *et al.* (2006): DQ137147–62, DQ13714765–6; Van Tuinen *et al.* (2000): AY158677, AY293618. **Cytochrome *b*:** Stanley & Harrison (1999): DQ137207–10, DQ137215–20, DQ13723–5, AF158250; Baker *et al.* (2006): DQ525761, DQ525766, DQ525776, NC_004538; Nunn *et al*. (1996): U48943, U48949, U48955; Nunn & Stanley (1998): AF076051–2, AF076046, AF076060, AF076062, AF076064, AF076068, AF076076, AF076089–90, U74335, U74350, U74353. **COI:** Nunn & Stanley (1998): DQ137167–72, DQ137174–86; Baker *et al.* (2006): DQ525781, DQ525786, DQ525796; Hebert *et al.* (2004): AY666477, AY666284; Kerr *et al.* (2007): DQ433048; Slack *et al.* (2006): NC_007172. **RAG-1:** Baker *et al.* (2006): DQ137230–3, DQ137235–47; Ericson *et al.* (2006): DQ881818, DQ881822.

Morphological character descriptions

List based on KF. Citations for the primary source of the characters are indicated with abbreviations as follows. A = Ando (2007); AH = Acosta Hospitaleche *et al.* (2007); BG = Bertelli & Giannini (2005); C = Clarke *et al.* (2007); CL = Clarke *et al.* (2010); GB = Giannini & Bertelli (2004); K = Ksepka *et al.* (2006); KC = Ksepka & Clarke (2010); KF = Ksepka *et al.* (2012); KT = Ksepka & Thomas (2011); OH = O'Hara (1986). Citation of Figures is also offered for some characters. Characters that are new or have been modified significantly from previous studies are indicated.

Integument

1. Tip of mandibular rhamphotheca, profile in lateral view: pointed (0); slightly truncated (1); strongly truncated, squared off (2); truncated but with a rounded margin (e.g., as seen in Procellariiformes) (3). (GB1)

2. Longitudinal grooves on the base of the culmen: absent (0); present (1). (GB2)

3. Longitudinal grooves on the base of latericorn and ramicorn: absent (0); present (1). (GB3)

4. Feathering of maxilla, extent: totally unfeathered (0); slightly feathered, less than half the length of maxilla (1); feathering that reaches half the length of maxilla (2); feathering surpassing half the length of maxilla (3). (GB4) **Ordered**

5. Ramicorn, inner groove at tip: absent (0); present and single (1); present and double (2). (GB5) **Ordered**

6. Orange or pink plate on ramicorn: absent (0); present (1). (GB6)

7. Plates of rhamphotheca, inflated aspect: absent (0); present (1). (GB7)

8. Gape: not fleshy (0); margin narrowly fleshy (1); margin markedly fleshy (2). (GB8) **Ordered**

9. Ramicorn color pattern: black (0); red (1); pink (2); yellow (3); orange (4); green (5); blue (6). (GB9)

10. Latericorn and ramicorn, light distal mark: absent (0); present (1). (GB10)

11. Latericorn color: black (0); red (1); orange (2); yellow (3); green (4); blue (5). (GB11)

12. Culminicorn color: black (0); red (1); orange (2). (GB12)

13. Maxillary and mandibulary unguis, color: black (0); red (1); yellow (2); green (3); blue-gray (4). (GB13)

14. Ramicorn, ultraviolet color spot (reflectance peak): absent (0); present (1). (KC14)

15. Bill of downy chick, color: dark (0); reddish (1); pale, variably horn to yellow (2); blue (3). (GB14)

16. Bill of immature, color: dark (0); bicolored red and black (1); red (2); yellow (3); gray (4). (GB15)

17. External nares: present (0); absent (1). (GB17)

18. Nostril tubes in adult: absent (0); present (1). (GB16)

19. Nostril tubes in hatchling: absent (0); present (1). (GB16)

20. External nares: well-separated (0); fused at midline (1). (KC19)

21. Iris color: dark (0); reddish-brown (1); claret red (2); yellow (3); white (4); silvery gray (5). (GB18)

22. Scale-like feathers: absent (0); present (1). (GB19)

23. Rhachis of contour feathers: cylindrical (0); flat and broad (1). (GB20)

24. Rectrices: form a functional fan (0); do not form a fan (1). (GB21)

25. Remiges: differentiated from contour feathers (0); indistinct from contour feathers (1). (GB22)

26. Apteria: present (0); absent (1). (GB23)

27. Molt of contour feathers: gradual (0); simultaneous (1). (GB24)

28. Yellow pigmentation in crown feathers (pileum): absent (0); present (1). (GB25)

29. Head plumes (crista pennae): absent (0); present (1). (GB26)

30. Head plumes (crista pennae), aspect: compact (0); sparse (1). (GB27)

31. Head plumes (crista pennae), aspect: directed dorsally (0); directed posteriorly, not drooping (1); directed posteriorly, drooping (2). (GB28)

32. Head plumes (crista pennae), position of origin: at base of bill close to gape (0); on the recess between latericorn and culminicorn (1); on forehead (2). (GB29) **Ordered**

33. Head plumes (crista pennae), color: yellow (0); orange (1). (GB30)

34. Nape (occiput), crest development: absent (0); slight (1); distinct (2). (GB31) **Ordered**

35. Periocular area, color: black (0); white (1); yellow (2); bluish gray (3). (GB32)

36. Fleshy eyering: absent (0); present (1). (GB33)

37. White eyering: absent (0); present (1). (GB34)

38. White eyebrow (supercilium): absent (0); narrow, from postocular area (1); narrow, from preocular area (2); wide, from preocular area (3). (GB35) **Ordered**

39. Loreal area (lorum), aspect: feathered (0); with spot of bare skin in the recess between latericorn and culminicorn (1); with spot of bare skin contacting eye (2); bare skin extending to the base of bill (3). (GB36) **Ordered**

40. Auricular patch (regio auricularis): absent (0); present (1). (GB37)

41. Throat pattern: black (0); white (1); yellow (2); irregularly streaked (3); with chinstrap (4). (GB38)

42. Collar: absent (0); at most slight notch present (1); present, diffusely demarcated (2); black, strongly demarked (3). (GB39) **Ordered**

43. Breast, golden in color: absent (0); present (1). (GB40)

44. Dorsum color: black (0); dark bluish gray (1); light bluish gray (2). (GB41)

45. Black marginal edge of dorsum between lateral collar and axillary patch, contrasting with dorsum: absent (0); present (1). (GB42)

46. Black dots irregularly distributed over white belly: absent (0); present (1). (GB43)

47. Flanks, dark lateral band reaching the breast: absent (0); present (1). (GB44)

48. Distinct dark axillary patch of triangular shape: absent (0); present (1). (GB45)

49. Flanks, extent of dorsal dark cover into the leg: incomplete, not reaching tarsus (0); complete, reaching tarsus (1). (GB46)

50. Rump: indistinct in color from dorsum (0); distinct white patch (1). (GB47)

51. Tail length: short, the quills barely emerge from the rump (0); quills distinctly developed (1). (GB48)

52. Outer rectrices, color: same as inner rectrices (0); lighter than inner rectrices (1). (GB49)

53. White line connecting leading edge of flipper with white belly: absent (0); present (1). (GB50)

54. Flipper, upperside, light notch at base: absent (0); present (1). (GB51)

55. Leading edge of flipper, pattern of upperside: black (0); white (1). (GB52)

56. Leading edge of flipper, pattern of underside: white (0); incompletely dark (1); completely dark and wide (2). (GB53)

57. Flipper, underside, dark elbow patch: absent (0); present (1). (GB54)

58. Flipper, underside, tip pattern: immaculate (0); patchy, in variable extent (1); small circular dot present (2). (GB55)

59. Immature plumage, white eyebrow (supercilium): absent (0); or present (1). (GB56)

60. Immature plumage, throat pattern (jugulum): black (0); or mottled (1); or white (2); or brown (3). (GB57)

61. Immature plumage, flanks, dark lateral band: absent (0); or present (1). (GB58)

62. Chicks hatch almost naked: no (0); yes (1). (GB59)

63. Dominant color pattern of first down: pale gray (0); distinctly brown (1); bicolored, dark above and whitish bellow (2); uniformly blackish gray (3). (GB60)

64. Dominant color pattern of second down: pale grey (0); distinctly brown (1); bicolored, dark above and whitish bellow (2); uniformly blackish gray (3). (GB61)

65. Chick, second down, collar: absent (0); present (1). (GB62)

66. Feet, dorsal color: dark (0); pink (1); orange (2); white-flesh (3); blue (4). (GB63)

67. Feet, soles distinctly darker than dorsal surface: absent (0); present (1). (GB64)

68. Feet, unguis digiti: flat (0); compressed (1). (BG65)

Reproductive Biology

69. Clutch size: two eggs (0); one egg (1). (GB65)

70. Incubatory sac: absent (0); present (1). (GB66)

71. Nest: no nest, incubation over the feet (0); nest placed underground, either burrowed in sand or inside natural hollow or crack (1); open nest, a shallow depression on bare ground or in midst of vegetation (2). (GB67)

72. Size of first egg relative to the second egg: similar (0); dissimilar, first smaller (1); dissimilar, second smaller (2). (GB68)

73. Crèche: absent (0); small, 3-6 birds (1); formed by dozens to hundreds of immatures (2). (GB69)

74. Eggs, shape: oval (0); conical (1); spherical (2). (BG71)

75. Ecstatic display: absent (0); present (1). (BG72)

Osteology

76. Premaxilla, tip (rostrum maxillare): pointed (0); weakly hooked (1); strongly hooked (2). **Ordered**. **NOTE**: In state 2, the tip ventrally exceeds the level of the tomial edge; whereas in state 1 the tip is approximately at the same level as the tomial edge. (GB0) (OH: fig.4)

77. Premaxilla, frontal process, naso-premaxillary suture: visible (0); obliterated (1). (BG95) (BG: fig.12)

78. Nasal cavity, external naris (cavum nasi, apertura nasi ossea), caudal margin respect the rostral margin of the hiatus orbitonasalis (fossa antorbitalia): overlapping each other (0); non overlapping (1). (OH5) (OH: fig.2; BG: fig.11)

79. Internarial bar (pila supranasalis), dorsal view: slender, slightly constricted laterally (0); wide throughout its length (1). (OH6) (OH: fig.3; BG: fig.12)

80. Internarial bar (pila supranasalis), shape in cross section: suboval (0); inverted U-shape (1). (C75)

81. Internarial bar (pila supranasalis), profile in lateral view (culmen): dorsal edge curves smoothly to tip of beak (0); pronounced step in dorsal edge (1). (KC78)

82. Tomial edge (crista tomialis), plane of tomial edge respect to the basitemporal plate (lamina parasphenoidalis): approximately at the same level (0); dorsal to the level of the basitemporal plate (1). (BG97)

83. Lacrimal: unperforated (0); perforated (1). (OH11) (OH: Fig.2; BG: Fig.11)

84. Lacrimal: reduced, concealed in dorsal view (0); small portion exposed in dorsal view (1); well-exposed in dorsal view (2). (BG82) **Ordered**

85. Lacrimal, contact with frontal: suture (0); fusion (1). (KT89)

86. Lacrimal, dorsal process: closely applied to the nasal (0); rostral arm of dorsal process separated from the nasal by a slit-like rostro-caudally elongate opening (1). This character originally referenced the frontal, however the actual separation occurs along the nasal-lacrimal contact (modified in KT90). (BG83)

87. Frontal, shelf of bone bounding salt-gland fossa (fossa glandulae nasalis) laterally: absent (0); present (1). (OH10) (BG: fig.9)

88. Squamosal, temporal fossa (fossa temporalis), size: fossae separated by considerable wide surface (at least the width of the cerebellar prominence) (0); more extensive, fossae meeting or nearly meeting at midline of the skull (1). (BG76) (BG: fig.9; K: fig.5)

89. Squamosal, temporal fossa (fossa temporalis), depth of caudal region: flat (0); shallow (1); greatly deepened (2). (BG77) (BG: fig.10) **Ordered**

90. Squamosal, development of the opening that transmits the a. ophthalmica externa in the caudoventral area of the temporal fossa (near nuchal crest): small or vestigial (0); well-developed (1). (BG78) (BG: fig.10)

91. Supraoccipital, paired grooves for the exit of v. occipitalis externae (sulcus vena occipitalis externae): poorly developed (0); deeply excavated (1). (BG74) (BG: fig.8)

92. Orbit, fonticuli orbitocraneales: small or vestigial (0); broad and conspicuous openings (1). (BG79) (BG: fig.10)

93. Ectethmoid: absent (0); weakly developed, widely separate from the lacrimal (1); well developed, contacting or fused to the lacrimal (2). (BG80)

94. Basioccipital, subcondylar fossa (fossa subcondylaris): absent or shallow (0); deep (1). (BG73) (BG: fig.7)

95. Basitemporal plate (lamina parasphenoidalis), dorsoventral position with respect to the occipital condyle: ventral to the level of the condyle (0); at the level of the condyle (1); dorsal to the level of the condyle, surface depressed (2). (BG86) **Ordered**

96. Basipterygoid process (proccessus basipterygoideus): absent (0); vestigial or poorly developed (1); well developed (2). (BG87) (BG: fig.7) **Ordered**

97. Eustachian tubes (tuba auditiva): open or very little bony covering near the caudal end of the tube (0); mostly enclosed by bone (1). (BG88) (BG: fig.7)

98. Pterygoid, shape: elongated (0); slight lateral expansion of rostral end (1) rostal end broad, pterygoid sub-triangular (2). (BG89) (BG: fig.7; KC: fig.22) **Ordered**

99. Palatine, lamella choanalis: curved and smooth plate, slightly differentiated from main palatine blade (0); ridged, distinct from main blade by a low keel (1); extended vertically ventrally forming the crista ventralis (2). (BG90) (BG: fig.13) **Ordered**

100. Vomer, laterally compressed, vertical laminae and free from palatines (0); horizontally flattened laminae and ankylosed with palatines (1). **NOTE**: This character defines a state 2 in KT98 and KF98. However, this state does not appear in any of the included taxa. (BG91) (BG: fig.13)

101. Facial foramen (foramen n. facialis): absent (0); present (1). (BG92)

102. Jugal arch, bar shape in lateral view: straight (0); slightly curved (1); ventrally bowed (2); strongly curved, sigmoid shape (3). (BG93) (BG: fig.14) **Ordered**

103. Jugal arch, dorsal process: absent (0); present (1). This pointed process is located on the caudal end of the jugal, adjacent to the condyle for articulation with the quadrate. (BG94)

104. Quadrate, relative lengths of otic and orbital processes (processus oticus and processus orbitalis): otic process longest (0); orbital process longest (1). (KC102)

105. Quadrate, otic process (processus oticus), rostral border, tubercle for m. adductor mandibulae externus, pars profunda: absent (0); present, as a ridge (1); presence, as a tubercle (2). (BG96) (BG: fig.15)

106. Quadrate, otic process (processus oticus), rostral border, tubercle for m. adductor mandibulae externus, pars profunda: contiguous with squamosal capitulum (0); separated from squamosal capitulum (1). (KC104) (KC: fig.23)

107. Quadrate, processus oticus, caudal margin in lateral view: straight (0); flexed so as to be concave caudally (1). (A9)

108. Mandible, symphysis: extensive bony connection (0); short terminal bony connection (1). (C101)

109. Mandible, posteriorly projected midline spur from dentary underlying symphysis: absent (0); present (1). (KC107)

110. Mandible, coronoid process (processus coronoideus), position on the dorsal margin of the mandible with respect to caudal mandibular fenestra (fenestra mandibulae caudalis): markedly rostral (0); on the rostral end of the fenestra (1); caudal to fenestra (2). (BG98) (BG: fig.16) **Ordered**

111. Mandible, rostral fenestra (fenestra mandibulae rostralis): imperforate or small opening (0); large opening (1). (OH8) (OH: fig.4; BG: fig.16)

112. Mandible, caudal fenestra (fenestra mandibulae caudalis): open, can be seen through from the medial or lateral aspects (0); nearly or completely concealed by the splenial medially (i.e., fenestra not visible in the medial aspect) (1). (OH9)

113. Mandible, mandibular ramus: depth subequal over entire ramus (0); pronounced deepening at midpoint (1). (BG101) (BG: fig.16)

114. Mandible, mandibular ramus: essentially straight or gently sloping (0); pronounced ventral deflection near midpoint (1). (KC112)

115. Mandible, dentary, length of dorsal edge relative to mandibular ramus length in lateral view: markedly more than half the length of ramus (0); approximately half the length of ramus (1). (BG103)

116. Mandible, articular, medial process (processus medialis): not hooked (0); hooked (1). (BG104) (BG: fig.17; K: fig.6)

117. Mandible, angular, aspect in dorsal view: sharply truncated caudally (0); caudally projected, forming retroarticular process (processus retroarticularis) (1). (BG106) (BG: fig.17)

118. Mandible, angular, retroarticular process (processus retroarticularis), aspect in dorsal view in relation to the articular area for the quadrate between the lateral and medial condyles (condylus lateralis and condylus medialis): broad, approximately equal to the articular area (0); moderately long, narrower than the articular area (1); very long, longer and narrower than the articular area (2). (BG105) (BG: fig.17) **Ordered**

119. Mandible, medial emargination between medial and retroarticular processes (processus retroarticularis and processus medialis): absent (0); weak concavity (1); strong concavity (2). (K108) (K: fig.6) **Ordered**

120. Atlas, processus ventralis: absent or slightly developed (0); well developed, high and prominent ridge on the dorsal surface of the arcus atlantis (1). (BG108) (BG: fig.18)

121. Transition to free cervicothoracic ribs begins at: 13th cervical vertebrae: (0); 14th cervical vertebrae (1); 15th cervical vertebrae (2). (BG109) **Ordered**

122. Cervical vertebrae, transverse process (processus transversus) in last five cervical vertebrae: not elongated laterally (0); greatly elongated laterally (1). (BG111)

123. Thoracic vertebrae, posteriormost vertebrae: heterocoelous (0); weakly opisthocoelous; (1); strongly opisthocoelous (2). (K114) **Ordered**

124. Thoracic vertebrae, deep excavation on lateral face of posterior thoracic vertebrae: absent (0); present (1). (KC124)

125. Synsacrum, number of incorporated vertebrae: nine (0); eleven (1); twelve (2); thirteen (3); fourteen (4), fifteen or more (5). (C117)

126. Synsacrum, height of crista synsacri between acetabuli: flat or weakly projected (0); strongly projected (1). (KC126)

127. Synsacrum, first incorporated vertebra, position of fovea costalis: caudal to level of processus transversus (0); cranial to level of transverse process (1). (KF229)

128. Synsacrum, ventral surface of first few incorporated vertebrae: rounded or flattened (0); sharp, blade-like ventral margin (1). (A63)

129. Caudal vertebrae: seven (0), eight (1), nine (2). (BG113) **Ordered**

130. Pygostyle, shape: tapers to a narrow edge both dorsally and ventrally as in most volant birds (0); triangular in cross-section with a wide, flat ventral margin (1). (KF232)

131. Thoracic ribs, uncinate processes (costae, processes uncinati): elongate, narrow (0), wide at base, spatulate (1), extremely wide at base (2). Reference to bifurcation of the processes in state 2 from previous formulations of this character has been removed, as bifurcation shows individual variation in all species of *Pygoscelis*. (BG114) (BG: fig.19)

132. Thoracic ribs, uncinate processes (costae, processes uncinati): fused to ribs (0); unfused (1) (KC129)

133. Sternum, external spine (spina externa rostri): absent (0); present (1). (OH13) (BG: fig.20)

134. Sternum, facies articularis furculae projects as a distinctive process: absent (0); present (1). (BG116) (BG: fig.20)

135. Sternum, articular facets for coracoids (sulcus articularis coracoideus): meet or overlap one another at midline (0); separated by wide non-articulatory surface (1). (C122) (BG: fig.20)

136. Sternum, orientation of sulcus articularis coracoideus in ventral view: sulci oriented in essentially straight horizontal line (0); sulci directed caudolaterally so as to together form an inverted U shape (1). (A15) (KF: fig.3)

137. Sternum, labrum internum: continues as sharp ridge onto the base of the spina externa (0); fades away without continuing onto the base (1). (C123)

138. Sternum, caudal incisurae: absent (0); two (1); four (2). (KC134)

139. Sternum, trabecula lateralis projects caudal to main body of sternum: no (0); yes (1). (KF234)

140. Furcula, hypocleidium (apophysis furculae): absent or low knob-like process (0); long, blade-like process (1). (BG117)

141. Furcula, ramus: sub-ovoid in cross-sectional omal end (0); mediolaterally flattened and craniocaudally expanded at omal end (1). (CL218)

142. Scapula, acromion: craniodorsally directed, nearly parallel to long axis of scapular shaft at apex (0); forms a blunt triangular projection with apex directed approximately at 45 degree angle from long axis of scapular shaft (1); narrow and tapering, apex omally directed (2); narrow and tapering, apex directed at a right angle to scapular shaft (3). **NOTE**: In KF136, only three states are defined. However, the matrix includes four states. Here the four states of that matrix are used. (CL223)

143. Scapula, facies articularis humeralis: rounded, projecting from shaft of scapula (0); compressed and ovoid, projecting from shaft of scapula (1); flattened and nearly merged with shaft of scapula (2). (KF235)

144. Scapula, blade, caudal half (corpus scapulae, extremitas caudalis): blade-like (0); slightly expanded (1); broadly expanded, paddle-shaped (2). (BG118) (KC: fig.24)

145. Coracoid, length: shorter than humerus (0); greatly elongated, longer than humerus (1). (KC137)

146. Coracoid, processus acrocoracoideus, region of tuberulum brachiale: craniocaudally compressed (0); craniocaudally expanded, with a large flat surface cranial to tuberulum brachiale. (A22)

147. Coracoid, scapular cotyle (scapula cotylaris): deep and socket-like (0); shallow depression (1). (CL217)

148. Coracoid, medial margin, coracoidal fenestra: complete (0); incomplete (1); absent (2). (OH14) (OH: fig.6; BG: fig.21; K: fig.7)

149. Coracoid, foramen nervi supracoracoidei: absent (0), present (1). Mayr (2005) cited ontogenetic evidence that this foramen is not homologous to the coracoidal fenestra of penguins. (K122)

150. Coracoid, sternal margin (extremitas sternalis coracoidei): greatly expanded (0); moderate expansion (1). (BG120) (BG: fig.21)

151. Coracoid, profile of the sternal margin (extremitas sternalis coracoidei) in ventral view: convex (0) concave (1), flat (2). **NOTE**: State 1 describes the strongly concave margin seen in *Gavia* and the slight concavity seen in *Aptenodytes*, whereas most penguins show a flatter margin and are consequently are coded as 2. This differs from the

code used by K124, KC141, KT143 and KF143, who use state 1 for all extant penguins. (K124) (K: fig.7; KC: fig.25)

152. Coracoid, lateral process (processus lateralis): absent or highly reduced (0); well-developed (1). (KC142)

153. Coracoid, facies articularis sternalis, dorsal surface: single facet (0); two facets (1). (KF236)

154. Forelimb elements: subcircular in cross section (0); flattened (1). (BG121)

155. Humerus, head: very developed and reniform, continuous with tuberculum dorsale: absent (0); present (1). (BG122)

156. Humerus, proximal edge of head in posterior view: semicircular humeral head with apex located near midline (0); humeral head with the shape of a rampant arch, with ventral apex, slightly prominent proximally (1); humeral head with the shape of a rampant arch with ventral apex, strongly prominent proximally (2). **NEW STATE**: State 1 refers to the degree of prominence seen in *Spheniscus*, whereas state 2 can be seen in *Pygoscelis*. Both states are included in state 1 of C132, KC145, KT147 and KF147. (C132)

157. Humerus, notch between the dorsal tubercle and humeral head: present (0); absent (1). **NEW CHARACTER**: This character is clearly visible in caudal view. State 0 can be seen in *Pygoscelis* and state 1 in *Spheniscus*. See Göhlich (2007).

158. Humerus, incisura capitis: essentially confluent with sulcus transversus (0); connected with the sulcus transversus trough a narrow sulcus (1); completely separated from sulcus transversus (2). **NEW STATE**: State 1 refers to the condition seen in *Palaeospheniscus patagonicus*, whereas state 2 can be seen in *Eudyptes*. This connection

is more subtle than in *Anthropornis* in which the transverse sulcus and capital incisure forms a single cranial sulcus (state 0). (K127) (K: fig.10)

159. Humerus, capital incisure: extends to secondary tricipital fossa (0); separated from secondary tricipital fossa (1). (CL222)

160. Humerus, pit for ligament insertion on proximal surface adjacent to head: absent or very shallow (0); deep (1). (K128) (K: fig.8)

161. Humerus, orientation of intumenscentia humeri and tuberculum ventrale: intumenscentia projects ventrally from shaft, tuberculum oriented posteriorly (0); intumenscentia projects ventrally from shaft, tuberculum oriented ventrally (1); intumenscentia projected more anteroventrally (so as to be partially obscured in posterior view), tuberculum oriented anteroventrally (2). (K129) (K: fig.10)

162. Humerus, proximal margin of tricipital fossa (fossa tricipitalis): weak projection (0); projects so as to be well-exposed in proximal view (1). (K135) (K: fig.8)

163. Humerus, proximal border of tricipital fossa in ventral view: concave proximal margin (0), straight to slightly concave border (1). **NOTE**: State 0 represents a truly concave margin as can be seen in *Madrynornis*; whereas state 1 includes the slightly concave margin usually present in *Palaeospheniscus* and the almost straight one present in *Spheniscus*. (KT154) (KT: fig.1m-o)

164. Humerus, tricipital fossa (fossa tricipitalis), aspect: small with penetrating pneumatic foramina (0); moderate fossa without pneumatic foramen (1); deep fossa without pneumatic foramen (2). (BG123)

165. Humerus, tricipital fossa (fossa tricipitalis): single (0); bipartite (1). (BG 124) (BG: fig.22)

166. Humerus, deltoid crest, impressio m. pectoralis: superficial poorly-defined groove (0); shallow, well-defined oblong fossa (1); deep, well-defined oblong fossa (2). **Ordered**. **NOTE**: In state 2, the deltoid crest is well defined distally, whereas in state 1 it is poorly defined. (BG125)

167. Humerus, impressio insertii m. supracoracoideus: small, semicircular scar (0); greatly elongated with long axis sub-parallel to main axis of humeral shaft (1). (K133) (K: fig.9)

168. Humerus, impressio insertii m. supracoracoideus and m. latissimus dorsi: separated by a wide gap (0); separated by a moderate gap (1); separated by small gap or confluent (2). (K134) (K: fig.9; KC: fig.26) **Ordered**

169. Humerus, coracobrachialis caudalis scar: clearly separated from head (0); scar contacts distal margin of head (1). (CL219)

170. Humerus, coracobrachialis caudal scar: deeply depressed, subcircular (0); flat, ovoid, oriented dorsoventrally (1); flat, elongate and oriented obliquely at approximately 45 degree angle to long axis of shaft (2). (CL220)

171. Humerus, groove for coracobrachialis nerve: absent or poorly defined (0); sharp, narrow sulcus (1). (CL221)

172. Humerus, shaft, dorsoventral width: shaft thins or maintains width distally (0); shaft widens distally (1). (K136) (K: fig.10)

173. Humerus, nutrient foramen (foramen nutricum): situated on ventral face of shaft (0) situated on anterior face of shaft (1). (C143)

174. Humerus, anterior face of shaft elongate depression near ventral margin: absent (0); present (1). (C144)

175. Humerus, shaft, sigmoid curvature: absent or weak (0); strong (1). (K137) (K: fig.10)

176. Humerus, shaft robustness index (proximodistal length / ventrodorsal width at middle point): greatly elongated, SRI ≥ 7 (0); greatly slender, 7 > SRI ≥ 6 (1); slender, 6 > SRI ≥ 5 (2); thick, 5 > SRI ≥ 4 (3); bulky, DRI < 4 (4). **NEW CHARACTER**: For this index, the proximodistal length is measured from the contact between the dorsal tubercle and humeral head (proximal end), to the contact between the ulnar condyle and the trochlear processes (distal end). The ventrodorsal width is measured at the middle point of the diaphysis, regardless of the position of the preaxial angle. State 0 can be seen in *Waimanu*, state 1 in *Perudyptes*, state 2 in *Palaeeudyptes*, state 3 in *Palaeospheniscus* and state 4 in *Pachydyptes*. (KC: fig.26)

177. Humerus, preaxial angle: absent or inconspicuous (0); well defined (1). **NEW CHARACTER**: Although there is a large quantitative variation in the development of this angle, its pattern of presence or absence is a stable character among many taxa. In state 0 the dorsal edge of the shaft is curved and without a clear preaxial angle, whereas in state 1 the angle creates a clear inflection point. State 0 can be seen in *Eudyptes* and state 1 in *Spheniscus.*

178. Humerus, development of dorsal supracondylar tubercle (processus supracondylar dorsalis): absent (0); compact tubercle (1); elongate process (2). (BG126)

179. Humerus, demarcation of sulcus scapulotricipitalis: not demarcated (0); passage a well-marked groove (1); development of trochlear ridge for articulation with os sesamoideum m. scapulotricipitis (2). (BG127). **Ordered**

180. Humerus, posterior trochlear ridge: extends beyond ventral margin of the humeral shaft (0); reaches the ventral margin (1); does not reach the ventral edge (2). **NEW STATE**: The new state 1 can be seen in *Palaeospheniscus* and *Eudyptes*. As a result, the ridge often slightly exceeds the ventral margin in cranial view but not in caudal view. (BG128) (BG: fig.23)

181. Humerus, scar for origin of m. brachialis: ovoid fossa on cranial face of humerus at distal end (0); proximodistally elongate scar on dorsal margin of humeral shaft, with diagonally oriented proximal border (1); proximodistally elongate scar on dorsal margin of humeral shaft, with chevron-shaped proximal border (2). (A34)

182. Humerus, angle between main axis of shaft and tangent of ulnar and radial condyles (condylus dorsalis and condylus ventralis): less than 35^{o} (0); 35° to 45^{o} (1); greater than or equal to 45^{o} (2); nearly 90^{o} (3). **NEW STATE**: The new state 0 can be seen in *Perudyptes* and *Anthropornis*. State 3 refers to the state in most flying birds, and state 2 represents values closer to 45 than to 90^{o}. States 0 and 1 were included in state 0 of KC141, KT169 and KF169. The values of angles for fossil taxa were obtained by photo analysis using TpsDIG version 2. (K141) (KC: fig.26)

183. Humerus, ulnar condyle (condylus ventralis): rounded condyle displaced over the anterior edge of the humerus (0); ulnar condyle almost parallel to the radial, slightly surpassing the anterior edge of the humerus (1); ulnar condyle almost parallel to the radial, not surpassing the anterior edge of the humerus (2). **MODIFIED**: Under this new definition, state 0 can be seen in *Palaeeudyptes,* state 1 in *Palaeospheniscus* and state 2 in *Spheniscus*. Although the anterior projection of the ulnar condyle in state 1 is less

pronounced than in state 0 (seen in the most basal penguins), it is more pronounced than in state 2. (K142) (K: fig.11)

184. Humerus, shelf adjacent to condylus ventralis: large, ratio of condyle width: shelf width >1.3 (0); moderate, ratio of condyle width: shelf width 1.3-2.0 (1); greatly reduced, less than half condyle width (2). (K143) (K: fig.11) **Ordered**

185. Radius, shaft: narrow (0); broad and flattened (1). (KC166)

186. Radius, proximally projecting spike-like process at cranial margin: absent (0); present (1). (KF239)

187. Ulna, olecranon position: arises at level of or proximally surpassing humeral cotylae (0); slightly distally displaced from cotylae (1); located one fourth of length to proximal end (2). **MODIFIED**: Because a combination of shapes and positions can be seen in penguins, we decided to separate both in two independent characters, previously coded together (K144). Under this new definition, state 0 can be seen in *Puffinus*, state 1 in *Icadyptes* and state 2 in *Spheniscus*. (K144) (K: fig.12; KC: fig.27)

188. Ulna, olecranon shape: short and robust (0); tab-like projection with a rounded posterior margin (1); tab-like projection with a squared posterior margin (2); tab-like projection with a distinctive angular posterior margin (3). **NEW CHARACTER**: Separation of the position and shape of the olecranon into two independent characters, previously coded together (K144). State 0 can be seen in *Puffinus*, state 1 in *Icadyptes*, state 2 in *Kairuku* and state 3 in *Spheniscus*. (K: fig.12; KC: fig.27)

189. Ulna, distinct process extending toward sulcus humerotricipitalis of humerus: absent (0), present (1). (K145)

190. Ulna incisura radialis: concave in proximal view, so that the ulna contacts the proximal radius at both its caudal and ventral surfaces (0); obsolete, so radius and ulna abut one another at a nearly flat contact (1). (KF240) (KF: fig.5g-h)

191. Ulnare: U-shaped (0); triangular, fan-shaped wedge (1). (KC169)

192. Ulnare, distal angle: rounded (0); pointed (1). **NOTE**: This character refers to the distal angle in the specialized fan-shaped ulnare of penguins and is considered non-comparable for outgroup taxa. (KF241)

193. Carpometacarpus, pisiform process (processus pisiformis): well-projected round tubercle (0); reduced to a low ridge (1). (C155)

194. Carpometacarpus, distal facet on metacarpal I: absent (0); present (1). (C156) (KC: fig.28)

195. Carpometacarpus, metacarpal II, distinct anterior bowing: absent (0); present (1). (C157)

196. Carpometacarpus, extension of metacarpals II and III: subequal or III slightly shorter (0); metacarpal III projects markedly distal of metacarpal II. (C158) (KC: fig.28)

197. Carpometacarpus, metacarpal III, distal articular surface (facies articularis digitalis major): wedge shaped or broadens anteriorly in distal view (0), slightly depressed ovoid surface (1). (C159)

198. Carpometacarpus, extensor process (processus extensorius): present (0); absent (1) (KC175)

199. Carpometacarpus, metacarpal II, distal expansion: absent (0); present (1). (KC176)

200. Phalanges of manus, phalanx digit III proximal process: absent (0); present (1). (BG130) (KC: fig.28)

201. Phalanges of manus, relative length of phalanx III-1 and phalanx II-1: phalanx III-1 shorter (0); subequal (1). (C161) (KC: fig.28)

202. Phalanges of manus, length relative to carpometacarpus: long (0); short (1). (BG131)

203. Fusion of ilia to synsacrum: unfused (0); partially fused (1); well-fused (2). (K149) (K: fig.13; KC: fig.29) **Ordered**

204. Pelvis, preacetabular ilia: approach one another, but do not contact at midline (0); contact at midline forming canalis iliosynsacralis (1). **NOTE**: This character defines three states in KC181, KT187 and KF187; however, state 0 does not appear in any of the included taxa. Consequently, we keep only states 1 and 2 described in those works, recoding them as 0 and 1 respectively. (KC181)

205. Pelvis, foramina intertransversalia large, forming wide openings on dorsal surface of pelvis: absent (0); present (1). (KC182)

206. Ilium, projected postiliac spine: absent (0); present (1).

207. Pelvis, size of foramen ilioischiadicum and foramen acetabuli: foramen ilioischiadicum smaller or similar in size (0); larger (1). (OH16) (BG: fig.24; KC: fig.29)

208. Pelvis, fenestra ischiopubica: very wide and closed at its caudal end (0); slit-like and open at its caudal end (1). (BG133)

209. Ischium, most caudal extent in relation to postacetabular ilium: ischium shorter than ilium (0); ischium projects slightly beyond the ilium (1); ischium produced far caudal to ilium (2). (BG134) (BG: fig.24)

210. Patella: absent or unossified (0); present (1). (KC187)

211. Patella, sulcus m. ambiens: shallow groove (0); deep groove (1); perforated (2). (BG135) (OH: fig.8; BG: fig.25)

212. Tibiotarsus, crista patellaris: slightly developed (0); moderate enlarged (1); greatly enlarged (2). (BG136) **NOTE**: In KC189, KF196 and KF195 only two states are defined. However, the matrices include three states. These are the three states used in their matrices.

213. Tibiotarsus, shaft, anteroposterior flattening: weak, midshaft anteroposterior depth greater than 75% mediolateral width (0); strong, midshaft anteroposterior depth equal to or less than 75% mediolateral width (1). (C169)

214. Tibiotarsus, notch in distal edge of medial condyle (condylus medialis): present (0); absent (1). (AH38)

215. Tibiotarsus, lateral condyle (condylus lateralis) in lateral profile: ovoid (0); subcircular (1). (AH37)

216. Tibiotarsus, sulcus extensorius: laterally positioned (0); close to midline (1); medially positioned (2). **NOTE**: Variation of this feature in penguins was noted by Clarke et al. (2003). (KC193).

217. Tibiotarsus, medial margin in distal view: margin is nearly straight (0); margin strongly convex (1). (KF242)

218. Tarsometatarsus, elongation index (proximodistal length / mediolateral width at proximal end): elongated, EI ≥ 3 (0); slender, 3 > EI ≥ 2.5 (1); shortened, 2.5 > EI ≥ 2 (2); greatly shortened, EI < 2 (3). **NEW STATE**: State 2 can be seen in *Palaeospheniscus* and *Eudyptula*; whereas the new state 3 can be seen in *Nucleornis* and

Aptenodytes. This latter state was included in state 2 of K156, KC194, KT200 and KF200. Values for some Antarctic fossils were obtained from the table of measurements in Myrcha et al. (2002). (BG138) **Ordered**

219. Tarsometatarsus, collateral lateral ligament scar (impressio lig. collat. lat.): absent or inconspicuous (0); well defined creating a depression over the lateral surface (1); well-defined creating a notch on the proximolateral vertex (2). **NEW CHARACTER**: State 0 can be seen in *Eudyptes*, state 1 in *Pygoscelis* and state 2 in *Spheniscus*.

220. Tarsometatarsus, medial margin, pronounced convexity: absent (0), present (1). (K157)

221. Tarsometatarsus, enclosed hypotarsal canals (canales hypotarsi): present (0); absent (1). (BG141)

222. Tarsometatarsus, relative plantar projection of medial and lateral hypotarsal crests: medial crest projects farther than lateral (0); projection of medial and lateral hypotarsal crests subequal (1). (KT203)

223. Tarsometatarsus, intermediate hypotarsal crests (crista intermediae hypotarsi): distinct and well defined in plantar view, separated by groove (0); united with lateral crest, slightly separated by shallow groove in proximal view (1); indistinguishable or absent (2). **NEW STATE**: Under this new definition, state 0 can be seen in *Mesetaornis*, the new state 1 in *Palaeospheniscus* and state 2 in *Spheniscus*. (K158) (K: fig.14-15)

224. Tarsometatarsus, lateral hypotarsal crest (crista lateralis hypotarsi): enlarged and connected with medial crest (0); well defined and parallel to proximodistal axis of tarsometatarsus (1); reduced, poorly defined and proximal to lateral foramen (2); forming a diagonal ridge that overhangs lateral foramen (3). **NEW CHARACTER**: State 0 can be

seen in *Gavia*, state 1 in *Thalassarche*, state 2 in *Pygoscelis* and state 3 in *Palaeospheniscus*.

225. Tarsometatarsus, crista medialis hypotarsi: present (0); absent (1). (KF243) (KF: fig.7l,p,r)

226. Tarsometatarsus, dorsal sulcus between metatarsals II and III (sulcus longitudialis dorsalis medialis): absent or barely perceptible (0); shallow groove (1); moderate groove (2) deep groove (3). (K159) (K: fig.15) **Ordered**

227. Tarsometatarsus, proximal vascular foramina on plantar surface: foramen vasculare proximale mediale present, foramen vasculare proximale laterale absent or vestigial (0); both foramina present (1); foramen vasculare proximale laterale present, foramen vasculare proximale mediale absent or vestigial (2). **NOTE**: State 1 refers to the plantar opening of the medial foramen; regardless if it is open at the plantar surface as in *Pygoscelis*, or at the medial surface of the medial hypotarsal crest as in *Spheniscus*. (K162) (K: fig.14-15; KC: fig.30)

228. Tarsometatarsus, medial hypotarsal crest (crista medialis hypotarsi) perforated by opening for the medial foramen proximalis vascularis: absent (0); present (1). (BG139) (BG: fig.26)

229. Tarsometatarsus, proximal vascular foramen lateral on dorsal surface: absent or vestigial (0); small (1); enlarged (2). **NEW CHARACTER**: Although there is a large quantitative variation in the size of the vascular foramina, the extreme morphologies described for states 0 and 2 are exclusive of some taxa. State 0 can be seen in *Eretiscus*, state 1 in *Eudyptes* and state 2 in *Spheniscus humboldti*.

230. Tarsometatarsus, opening for medial foramen proximalis vascularis distal to crista medialis hypotarsi: absent (0); present (1). **NOTE**: Because both this opening and an additional opening perforating the crista medialis hypotarsi can be present in *Aptenodytes,* they are treated as independent characters. (BG140)

231. Tarsometatarsus, distal vascular foramen (foramen vasculare distale): present, separated from incisura intertrochlearis lateralis by osseous bridge (0); present, open distally (1); absent (2). (K163) (K: fig.15; KC: fig.30) **Ordered**

232. Tarsometatarsus, os metatarsale IV: distal end projects laterally (0); straight (1), distal end deflected medially (2). (K 160)

233. Tarsometatarsus, intertrochlear notches (incisura intertroclear): medial notch absent (0); medial notch deeper than lateral (1); sub-equal to equal deepness (2); lateral notch deeper than medial (3). **NEW CHARACTER**: This character is clearly visible in plantar view. State 0 can be seen in *Gavia,* state 1 in *Puffinus*, state 2 in *Aptenodytes* and state 3 in *Eudyptes*.

234. Tarsometatarsus, trochleae metatarsi II and IV in dorsal view: trochlea II shorter than IV (0); trochlea IV slightly shorter than II (1); equal (2). **NEW CHARACTER**: State 0 can be seen in *Gavia*, state 1 in *Eudyptes* and state 2 in *Spheniscus*.

235. Tarsometatarsus, trochleae in distal view: trochleae metatarsi III and IV aligned in same plane (0); trochlea metatarsi IV displaced dorsally (1). (KT211) (KT: fig.1w-y)

236. Tarsometatarsus, trochlea metatarsi II strongly plantarly deflected in distal view: no (0); yes (1). **NOTE**: This character refers to the plantar edge of the trochlea II with respect to the plane defined by the most plantar point of the trochleae III and IV in distal view; or with respect to the plane defined by the trochlear ridges of the trochlea III when

the trochlea IV is strongly dorsally deflected. State 0 can be seen in *Eudyptes* and state 1 in *Palaeospheniscus*. (A73)

237. Pedal digit I: small, with metatarsal I and single phalanx both present (0); metatarsal I reduced to an ossicle, claw represented by a minute ossicle or lost (1); metatarsal I absent (2).**NOTE**: Codings for Procellariiformes follow Forbes (1882); see also discussion in Mayr (2009). (KF245) **Ordered**

Myology

238. M. latissimus dorsi, pars cranialis, accessory slip: absent (0); present (1). (BG143)

239. M. latissimus dorsi, pars cranialis and pars caudalis: separated (0); fused (1). (BG144)

240. M. latissimus dorsi, pars metapatagialis, development: wide (0); intermediate (1); narrow (2). (BG145) **Ordered**

241. M. serratus profundus, cranial fascicle: absent (0); present (1). (BG146)

242. M. deltoideus, pars propatagialis, subdivision in superficial and deep layers: undivided (0); divided (1). (BG147)

243. M. deltoideus, pars major: triangular or fan-shaped (0); strap-shaped (1). (BG148)

244. M. deltoideus, pars major, caput caudale: short (0); intermediate (1); long (2). (BG149) **Ordered**

245. M. deltoideus, pars minor, origin on the clavicular articulation of the coracoid: absent (0); present (1). (BG150)

246. M. ulnometacarpalis ventralis: absent (0); present (1). (BG151)

247. M. iliotrochantericus caudalis: narrow (0); wide (1). (BG152)

248. M. iliofemoralis, origin: tendinous (0); partially tendinous and partially fleshy (1); totally fleshy (2). **NOTE:** This character previously included four states. The states 'mostly tendinous' and 'mostly fleshy' were lumped into a single state to avoid overweighing this ordered character. (BG153) **Ordered**

249. M. flexor perforatus digitis IV, rami II-III: free (0); fused (1). (BG154)

250. M. flexor perforatus digitis IV, rami I-IV: free (0); fused (1). (BG155)

251. M. flexor perforatus digitis IV, insertion of middle rami: on phalanx 3 (0); on phalanx 4 (1). (BG156)

252. M. latissimus dorsi, pars caudalis, additional origin from dorsal process of vertebrae: absent (0); present (1). (BG157)

Other soft tissue

253. Oral mucosa (bucca, tunica mucosa oris), buccal papillae group on the medial surface of the lower jaw (ramus mandibularis) at the level of the rictus: small number of rudimentary papillae with no clear arrangement (0); two clear rows of short conical papillae (1); large, elongated papillae with no clear arrangement (2). (BG158)

254. Tracheal rings: single (0); bifurcated (1). (KC219)

Consensus trees

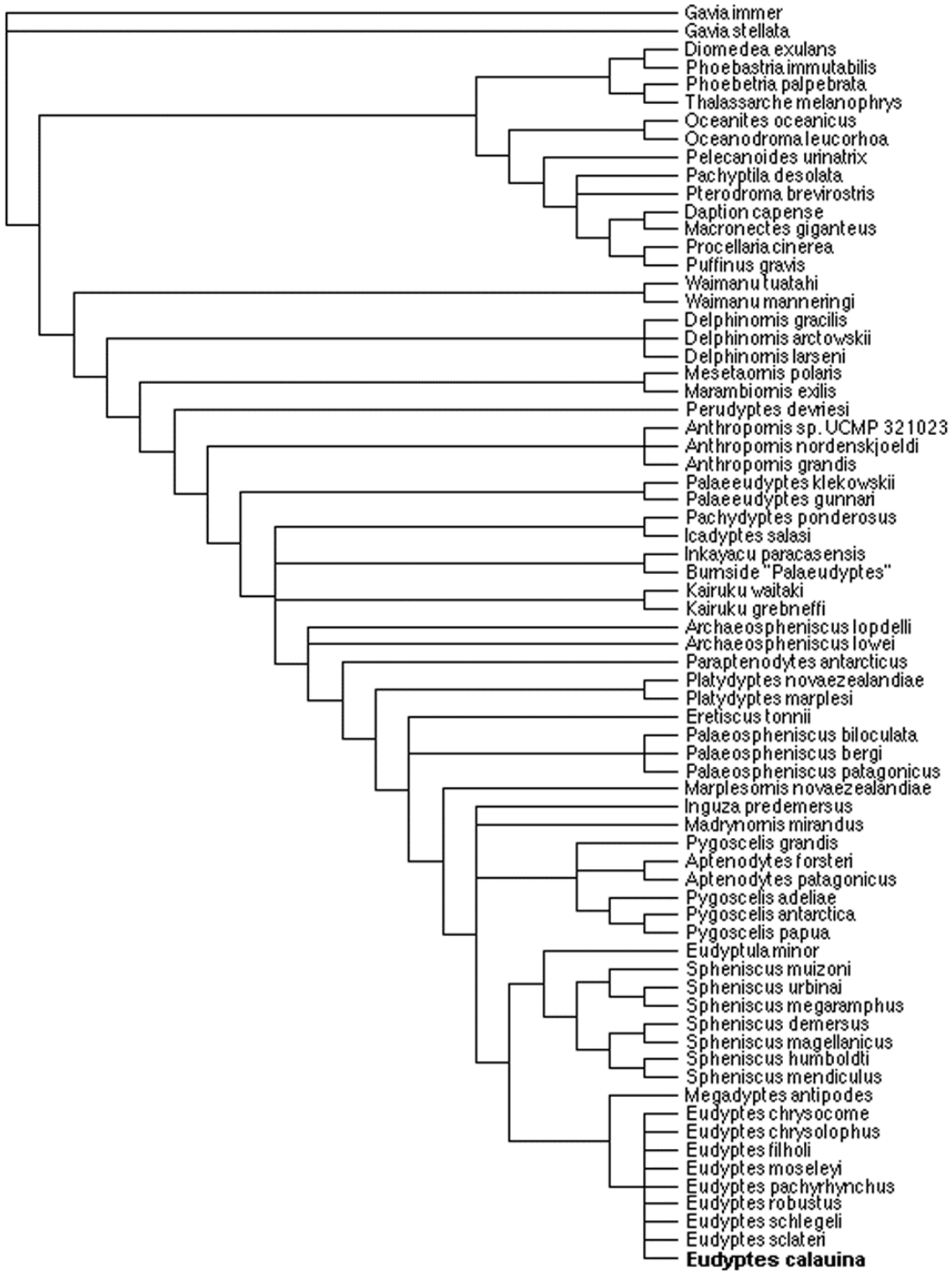

Figure S3.1. Combined analysis strict consensus. Strict consensus tree of 192 MPTs (tree length = 5563 steps, rescalated consistency index [RC] = 0.373, retention index [RI] = 0.699) from a combined analysis of morphological characters plus >6000 bp.

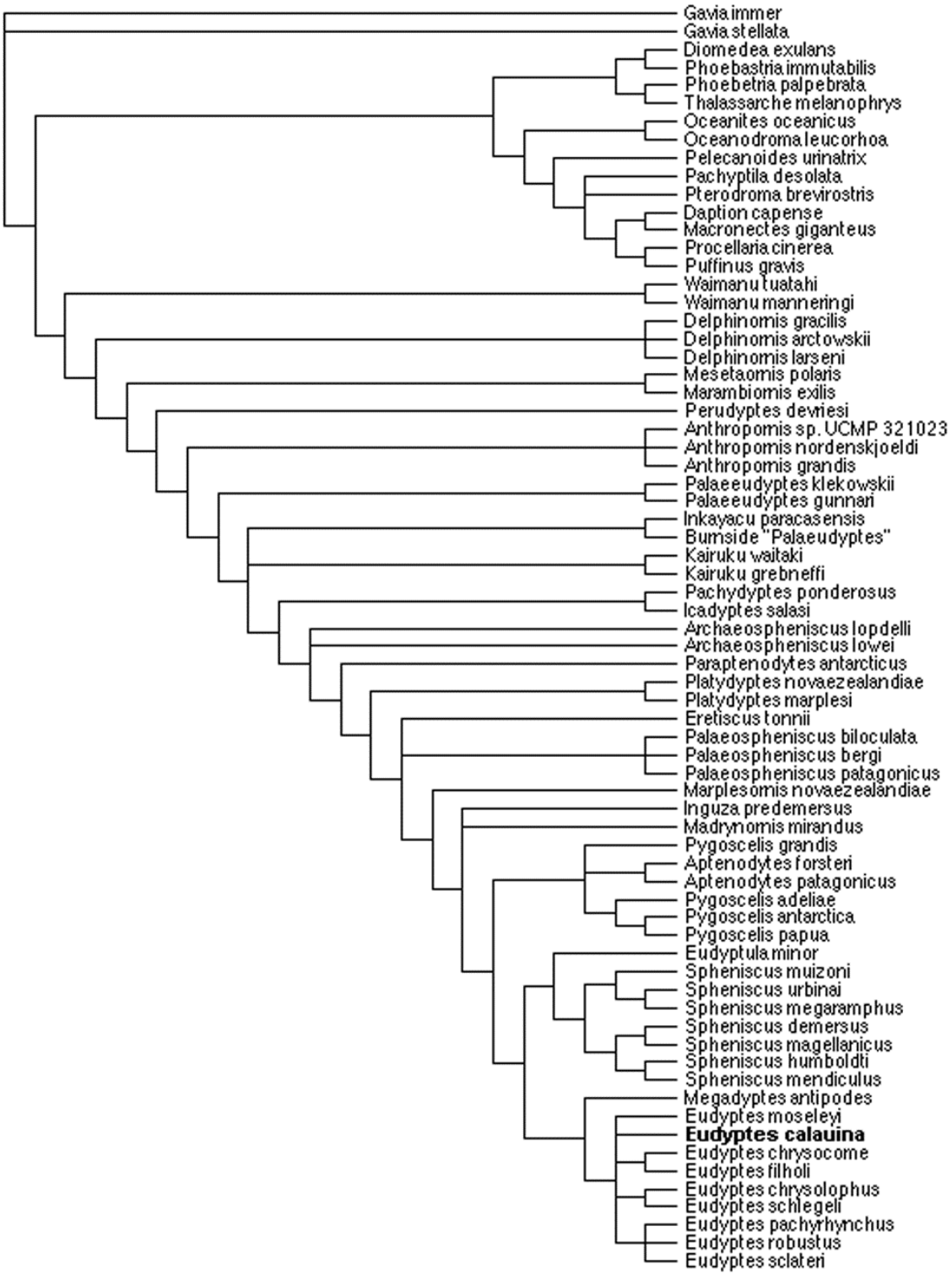

Figure S3.2. Combined analysis Adams consensus. Adams consensus tree of 192 MPTs (tree length = 5563 steps, RC = 0.373, RI = 0.699) from a combined analysis of morphological characters plus >6000 bp.

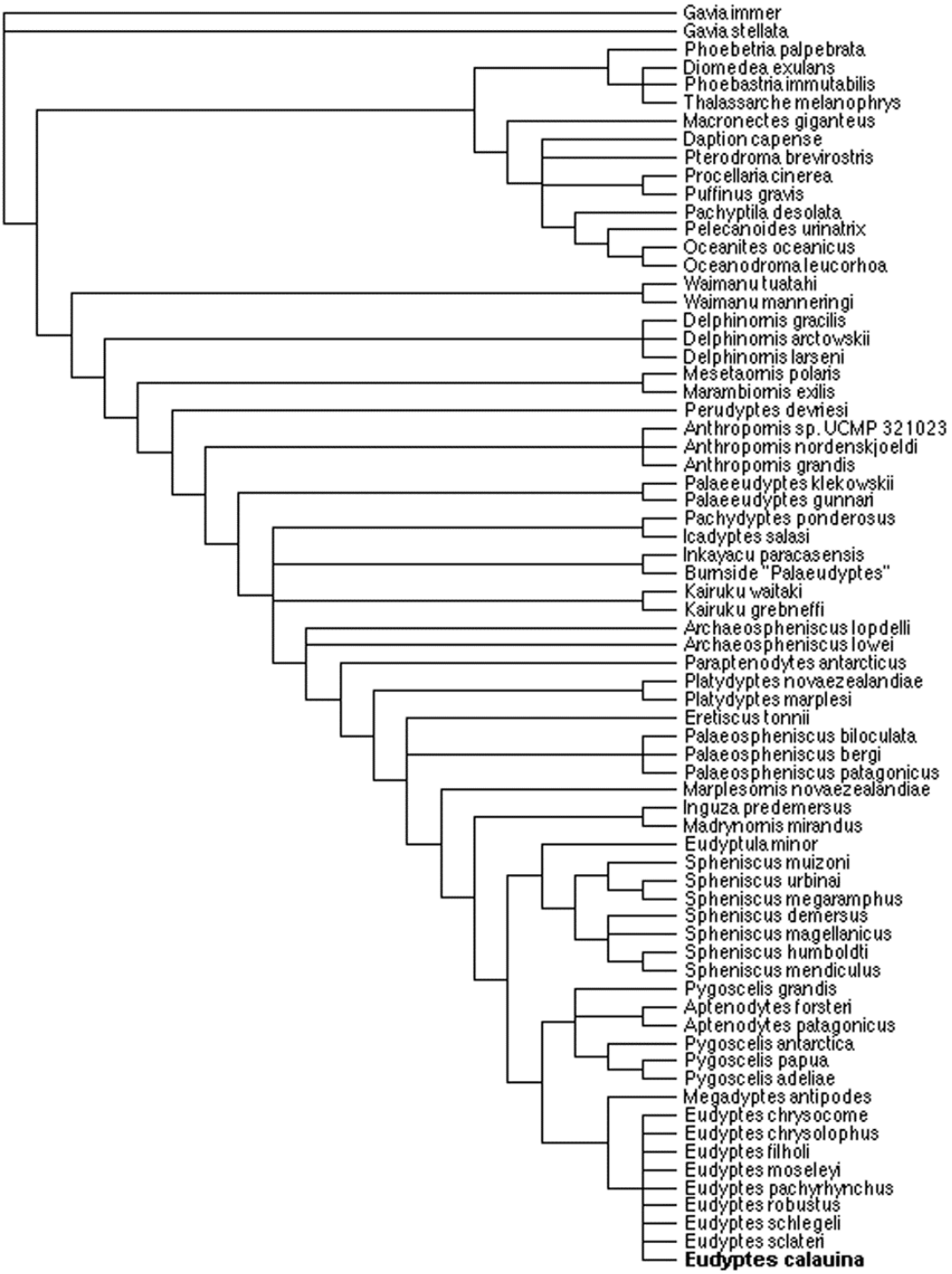

Figure S3.3. Morphology-only analysis strict consensus. Strict consensus tree of 704 MPTs (tree length = 802 steps, RC = 0.492, RI = 0.879) from an analysis of 254 morphological-only characters.

Figure S3.4. Morphology-only analysis Adams consensus. Adams consensus tree of 704 MPTs (tree length = 802 steps, RC = 0.492, RI = 0.879) from an analysis of 254 morphological-only characters.

List of osteological synapomorphies

Osteological synapomorphies (unambiguous and supportive) for main clades and genera monophyly, obtained from the combined analysis.

Clade/Taxa	**Unambiguous synapomorphies**	**Supportive synapomorphies**
Mesetaornis + *Marambiornis*	218(0)	—
Palaeeudyptes	—	157(0); 189(1)
Inkayacu + Burnside "*Palaeeudyptes*"	169(0); 171(1)	77(0); 140(1); 180(0); 236(1)
Pachydyptes + *Icadyptes*	177(0)	109(1); 157(0)
Palaeospheniscus	223(1); 236(1)	126(1); 127(0); 133(2); 163(1); 180(1)
Spheniscidae + *Madrynornis* + *Inguza*	88(0); 99(0); 106(1); 116(1); 119(2); 137(1)	98(2); 110(1); 118(1)
Spheniscidae excluding *Madrynornis* and *Inguza*	103(1); 136(0); 147(1); 224(2)	77(0); 105(1); 103(1); 158(2); 177(1)
Antarctic clade	83(0); 89(1); 90(1); 148(1); 151(1); 218(3); 219(1); 230(1)	102(3); 118(0); 211(0); 228(0); 233(2)
Aptenodytes	92(1); 111(1); 126(1); 133(0); 186(0); 219(0)	101(1); 120(1); 158(1)
Pygoscelis	84(1); 87(1); 115(1); 119(1); 203(1); 222(1)	160(0); 211(2)
Temperate-Tropical clade	226(2)	82(0); 180(1)
Burrowing clade	99(1); 102(1); 129(2); 156(1); 157(1); 226(3)	105(2); 207(1)
Eudyptula	125(3); 148(1); 176(2); 236(1)	177(0)
Pan-*Spheniscus*	78(1); 79(1); 80(1); 88(1); 110(0); 126(1); 163(1)	84(0)
Stem *Spheniscus*	136(1); 147(0)	207(0)
Crown *Spheniscus*	115(1); 118(2); 162(1); 235(1)	—
Yellow-headed clade	87(1); 91(0); 110(2); 115(1); 219(0)	112(1)
Megadyptes	—	233(2)
Eudyptes	102(3); 113(1); 218(3); 224(3); 234(1)	105(2); 177(0)

Additional References

Acosta Hospitaleche C, Gasparini G (2007) Evaluation for systematic purposes of the tarsometatarsal characters in Spheniscidae. Ornitologia Neotropical 18: 277-284.

Acosta Hospitaleche C, Tambussi C, Donato M, Cozzuol M (2007) A new Miocene penguin from Patagonia and its phylogenetic relationships. Acta Palaeontologica Polonica 52: 299- 314.

Baker AJ, Pereira SL, Haddrath OP, Edge A (2006) Multiple gene evidence for expansion of extant penguins out of Antarctica due to global cooling. Proceedings of the Royal Society B 217: 11–17

Banks J, Van Buren A, Cherel Y, Whitfield JB (2006) Genetic evidence for three species of rockhopper penguins, *Eudyptes chrysocome*. Polar Biology 30: 61-67.

Bertelli S, Giannini N P (2005) A phylogeny of extant penguins (Aves: Sphenisciformes) combining morphology and mitochondrial sequences. Cladistics 21: 209-239.

Clarke JA, Ksepka DT, Salas-Gismondi R, Altamirano AJ, Shawkey MD, *et al*. (2010) Fossil evidence for evolution of the shape and color of penguin feathers. Science 330: 954-957.

Clarke JA, Ksepka DT, Stucchi M, Urbina M, Giannini N, *et al*. (2007) Paleogene equatorial penguins challenge the proposed relationship between biogeography, diversity, and Cenozoic climate change. Proceedings of the National Academy of Sciences of the United States of America 104**:** 11545-11550.

Cooper A, Penny D (1997) Mass Survival of Birds across the Cretaceous- Tertiary Boundary: Molecular Evidence. Science 275: 1109–1113.

Ericson PGP, Anderson CL, Britton T, Elzanowski A, Johansson US, *et al.* (2006) Diversification of Neoaves: integration of molecular sequence data and fossils. Biology latters 2: 543-547.

Giannini NP, Bertelli S (2004) Phylogeny of extant penguins based on integumentary and breeding characters. Auk 121: 422-434.

Göhlich U (2007) The oldest fossil record of the extant penguin genus *Spheniscus*, a new species from the Miocene of Peru. Acta Palaeontologica Polonica 52: 285–298.

Guinard G, Marchand D, Courant F, Gauthier-Clerc M, Le Bohec C (2010) Morphology, ontogenesis and mechanics of cervical vertebrae in four species of penguins (Aves: Spheniscidae). Polar Biology 33: 807-822.

Hebert PDN, Stoeckle MY, Zemlak TS, Francis CM (2004) Identification of Birds through DNA Barcodes. PLoS Biol 2: e312.

Kerr KCR, Stoeckle MY, Dove CJ, Weigt LA, Francis CM, *et al*. (2007) Comprehensive DNA barcode coverage of North American birds. Molecular Ecology Notes 7: 535–543.

Ksepka DT, Bertelli S, Giannini NP (2006) The phylogeny of the living and fossil Sphenisciformes (penguins). Cladistics 22: 412-441.

Nunn GB, Stanley SE (1998) Body size effects and rates of cytochrome b evolution in tube-nosed seabirds. Molecular Biology and Evolution 15: 1360-1371.

Nunn GB, Cooper J, Jouventin P, Robertson CJR, Robertson GG (1996) Evolutionary relationships among extant albatrosses (Procellariiformes: Diomedeidae) established from complete cytochrome-b gene sequences. Auk 113: 784-801.

Paterson AM, Wallis GP, Gray RD (1995) Penguins, petrels, and parsimony: does cladistic analysis of behavior reflect seabird phylogeny? Evolution 49: 974-989.

Slack KE, Jones CM, Ando T, Harrison GL, Fordyce RE, *et al*. (2006) Early Penguin Fossils, plus Mitochondrial Genomes, Calibrate Avian Evolution. Molecular Biology and Evolution 23: 1144-1155.

Stanley SE, Harrison RG (1999) Cytochrome b evolution in birds and mammals: an evaluation of the avian constraint hypothesis. Molecular Biology and Evolution 16: 1575-1585.

Stephan B (1979) Vergleichende Osteologie der Pinguine. Mitteilung aus dem Zoologischen Museum in Berlin 55: 3- 98.

Van Tuinen M, Sibley CG, Hedges SB (2000) The Early History of Modern Birds inferred from DNA Sequences of Nuclear and Mitochondrial Ribosomal Genes. Molecular Biology and Evolution 17: 451-457.

Worthy TH (1997) The identification of fossil *Eudyptes* and *Megadyptes* bones at Marfells Beach, Marlborough, South Island. New Zealand Natural Sciences 23: 71-85.